Spring 5-2024

Analysis of Nonsmooth Neural Mass Models

Cadi Howell
University of Maine - Main, cadi.howell@maine.edu

Analysis of Nonsmooth Neural Mass Models

by

Cadi Howell

A Thesis Submitted in Partial Fulfillment
of the Requirements for a Degree with Honors
(Mathematics)

The Honors College

University of Maine

May 2024

Advisory Committee:
Peter Stechlinski, Associate Professor of Mathematics, Advisor
David Hiebeler, Professor of Mathematics and Statistics
Benjamin King, Professor of Molecular and Biomedical Sciences
Jane Wang, Assistant Professor of Mathematics and Statistics

ABSTRACT

Neural activity in the brain involves a series of action potentials that represent "all or nothing" impulses. This implies the action potential will only "fire" if the membrane potential is at or above a specific threshold. The Wilson-Cowan neural mass model [6, 28] is a popular mathematical model in neuroscience that groups excitatory and inhibitory neural populations and models their communication. Within the model, the on/off behavior of the firing rate is typically modeled by a smooth sigmoid curve. However, a piecewise-linear (PWL) firing rate function has been considered in the Wilson-Cowan model in the literature (e.g., see [5]). This function, however, is nonsmooth, and cannot be analyzed using standard mathematical theory. In this thesis, we considered the Wilson-Cowan neural mass model using a nonsmooth PWL firing rate function and analyze its behavior using techniques from generalized derivatives theory. To accomplish this, we calculated the sensitivities of the model parameters in order to determine the parameters that most impact the dynamics of the model across a set of parameter values. We also determined the stability of the model to better understand the long-term behavior of the model. We then compared the results of these analyses to that of the Wilson-Cowan model with a smooth firing rate function.

ACKNOWLEDGEMENTS

Thank you to my family for supporting me over the course of my time at the University of Maine. My parents, Gareth and Andrea, and my siblings, Megan and Ieuan, have motivated me to be the hard working person I am today. I am forever grateful for their encouragement and I strive to continue to make them proud.

I would also like to thank my advisor, Professor Peter Stechlinski, for his help throughout the entirety of this project. His support has made this process enjoyable, which has enhanced my love for math and sparked my interest in neuroscience.

In addition, I would like to acknowledge Professor Jane Wang, Professor David Hiebeler, and Professor Ben King for being members of my committee, as well as Professor Sue Ann Campbell and Professor Wilten Nicola for sharing their extensive knowledge on the topic of neural mass models with me.

Finally, I would like to thank the College of Liberal Arts and Sciences (CLAS) as they generously funded the beginnings of this project, allowing it to flourish into the following thesis.

TABLE OF CONTENTS

LIST OF FIGURES

LIST OF TABLES

CHAPTER I

INTRODUCTION

The brain can be described as an intricate network of 50 billion neurons, each with 7 thousand axon terminals, that are activated or deactivated by signals passed between neurons [6]. These signals are known as "action potentials", which can be described as “all or nothing impulses”. Given the complexity of the brain, it is clear to see that the creation of models for such a vast array of activity would prove to be difficult; however, modeling such behavior would provide information on neural behavior and further research on brain function. There have been many studies on mathematical neural mass models in an attempt to do such a thing.

The aim of a “mean field" neural mass model is to capture the change in firing rates involved in an array of neurons (i.e. a neural network) in a specific location of the brain [27]. Different models consider different aspects of a neural network, such as neuron types or ion channels. For example, in [29], a neural mass model is built based on three neuron population types: excitatory, inhibitory, and pyramidal neurons. Each of these neurons is defined by its function in the brain. An action potential that is generated by excitatory neurons triggers an action potential in a receiving neuron with the release of the neurotransmitter glutamate, while an action potential generated by inhibitory neurons prevents one in the receiving neuron with the release of the neu-

rotransmitter GABA [26]. Pyramidal neurons are one of the most common excitatory neurons [2], thus the model created in [29] groups them on their own. The authors of [14] follow a different neural mass model, which considers the synaptic reversal potential of ion channels, which is the necessary potential to result in a net ion channel current of zero. Another neural mass model is the θ-neuron model, which considers a network of θ-neurons and models the dynamics in synchronous, spiking, and periodic states [15]. Each neural mass model can be applied to different areas of the brain and model specific scenarios based on how well the model's considered aspects align with the biological phenomena present.

The Wilson-Cowan model [28] is a popular neural mass model following the dynamics of neural activity through ordinary differential equations (ODEs). This model considers a population of excitatory neurons and a population of inhibitory neurons and models the relationship between the two [5]. The simplest form of the Wilson-Cowan model is the "minimal network model", which considers the two populations with respect to aspects such as their firing rates and synapse weights. More complicated versions of the model consider the distance between neurons throughout the network, such as the "spatially structured model" [13]. Forms of the Wilson-Cowan model have been used previously in a number of cortical modeling studies to inform targeted research on visual hallucinations, epilepsy, the cognitive dynamics of movement, interpretation of neuroimaging data, and more [3].

As in several popular neural mass models, the Wilson-Cowan model utilizes a smooth "sigmoid" function to model the firing rate of neurons within a neural network. The smoothness of the function indicates that the right-hand side functions of

the model's equations are differentiable. Since derivative information can provide details on the dynamics of a model, this implies that analyses of such dynamics can be completed through standard methods. A background of smooth neural mass models including the Wilson-Cowan model can be found in [27, 7]. As popular as it is, the use of the sigmoid function to represent the firing rate of neurons is not necessarily biophysically motivated [3], which is a topic of discussion throughout this thesis. Thus a smooth firing rate function may not be the best choice to apply to the Wilson-Cowan model. However, applying nonsmooth functions implies standard theories of analysis may fail, thus research continues to be carried out using both forms of firing rate functions.

Analyses of nonsmooth (i.e. nondifferentiable but continuous) and discontinuous neural mass models have been completed by other authors. In [17], a mean field neural mass model with discontinuous right-hand functions is built by the reduction of a full network model to better analyze its behavior. This reduction allowed the authors to perform a stability and bifurcation analysis in [18] using a combination of smooth and nonsmooth theories. In another study, the authors of [5] consider a nonsmooth piecewise linear (PWL) function as well as a discontinuous step function (namely the Heaviside function) to represent the firing rate of the Wilson-Cowan model. They perform a stability analysis of the minimal and spatially structured models by applying Floquet theory to investigate the model with the PWL firing rate and find an unstable equilibrium point surrounded by a stable limit cycle. However, the linearization achieved through Floquet theory breaks down when the Heaviside function is used, therefore an adaptation is made to analyze the stability of the model.

The Heaviside function is used by authors to represent the firing rate of the Wilson-Cowan neural mass model as there are arguments that suggest it is more representative of biological phenomena. For example, in [10], they perform a bifurcation analysis of the Wilson-Cowan model using the Heaviside function. When comparing their results to the stability of the model with smooth and PWL firing rate functions, they find that the bifurcations of the models do not align. Although studies have been completed using discontinuous techniques, such discontinuous ODE functions are more complicated to mathematically analyze and it is generally more difficult to apply such tools in comparison to those developed for smooth models. Research on methods available for discontinuous neural mass models can be found in the references of [10].

On the other hand, authors have made developments in nonsmooth analysis and generalized derivatives theory [1], making it possible to analyze the Wilson-Cowan model and other variants with continuous but nonsmooth firing rate functions in a similar way to their smooth counterparts. Lexicographic directional derivatives [12], built from lexicographic differentiation [16], is one way in which such nonsmooth functions can be analyzed. This technique allowed Khan and Barton to develop a sensitivity theory [11] that can be applied to nonsmooth ODEs with right-hand side functions that are nonsmooth but continuous by characterizing local first-order generalized derivative information of the ODE solution with respect to the parameters of the system. Results of this theory are computationally relevant to nonsmooth numerical methods that require Clarke generalized derivative elements [4].

The theories discussed above can be utilized when analyzing the dynamics of neural mass models that are represented by nonsmooth equations, such as the Wilson-

Cowan model with a nonsmooth firing rate function. Such analyses may include a sensitivity analysis of a model, which determines the parametric influence to the model, where highly influential parameters greatly alter its dynamics when such parameter values are varied. As discussed above, many authors have studied the stability of neural mass models, which determines the long-term behavior of the state variables and provides information about the equilibria and limit cycles of a model. Both of these analysis techniques are topics explored in this thesis.

We will begin by introducing the mathematical background of nonsmooth ODE analysis in Chapter II. The formulation of the Wilson-Cowan model will follow in Chapter III, where we will discuss the model as an ODE system, explain the possible smooth and nonsmooth firing rate functions, and describe the state variable behavior. Next, the main contributions of this thesis are given, beginning with a local and nonlocal sensitivity analysis that is performed on the nonsmooth model in Chapter IV, during which we will determine the most influential parameter. We will then compare the results of this analysis to that of the sensitivity analysis of the smooth model. Then, in Chapter V, we will calculate the invariant sets of the nonsmooth model and determine their stability. Once again, after this analysis we will compare the results to those of the smooth model. Finally, in Chapter VI, we will draw conclusions about the smooth and nonsmooth models based on our findings and hypothesize biological implications for the results.

CHAPTER II

BACKGROUND

Analysis of Smooth ODE Systems

The material of this subsection has been adapted from [20], unless cited otherwise. Models of neural networks are made up of ordinary differential equations (ODEs), which are equations that define the relationship between unknown variables and their derivatives (also defined as instantaneous rates of change). The realm of differential equations can be broken up into two categories: ODEs and partial differential equations (PDEs). ODEs involve the derivative of an equation with respect to one independent variable, whereas PDEs involve derivatives with respect to multiple independent variables. A group of multiple ODEs is a system of ODEs and can be represented as follows:

$$\begin{aligned} \dot{x}(t) &= f(p, x(t)), \\ x(t_0) &= f_0(p), \end{aligned} \tag{1}$$

for the initial time, t_0, and initial conditions (ICs), $x(t_0)$, as well as the right-hand side function

$$f(p, x) = (f_1(p, x), \ldots, f_n(p, x)),$$

such that $f : D_p \times D_x \to \mathbb{R}^n$ and $f_0 : D_p \to D_x$ for the open and connected sets $D_p \subseteq \mathbb{R}^m$ and $D_x \subseteq \mathbb{R}^n$ where $x = (x_1, x_2, \ldots, x_n)$ is the vector of state variables and $p = (p_1, p_2, ..., p_m)$ is the vector of problem parameters. Here, $x(t)$ is called a solution of the ODE system in equation (1) on some interval $T \subseteq \mathbb{R}$ containing t_0 if it is differentiable for all time $t \in T$, $x(t) \in D_x$ for all $t \in T$, and $x(t)$ satisfies $\dot{x}(t) = f(p, x(t))$ for $t \in T$ and $x(t_0) = f_0(p)$ for some $p \in D_p$.

An important distinguishing factor of an ODE system is if the right-hand side functions of the ODEs are made up of smooth functions or not. Here, the term "smooth" indicates the function is C^1, which means it is differentiable and its derivative is continuous for each point $x \in D_x$. If the right-hand side functions of the ODE system are linear, the solution of the model can be found analytically. However, if these functions are nonlinear, it is more difficult to analytically find the solution and therefore more difficult to analyze the dynamics of the ODE system. Two methods of analyzing the dynamics of a nonlinear ODE system indirectly are a sensitivity and stability analysis. These methods of analysis can be completed using classical theory if all right-hand side functions are smooth.

The sensitivity of a model informs us on how much change occurs to the behavior of the states due to a perturbation of a parameter. If varying one parameter has a higher impact on the state behavior than another, the model is more sensitive to this parameter. To investigate this idea, a sensitivity analysis can be performed. Classical sensitivity theory requires the calculation of a set of equations, the sensitivity equations, which can then be solved to recover the sensitivity functions. For reference value $p = p_0$ and corresponding ODE system solution $x(t) = x(t, p_0)$, the sensitivity functions are

calculated by,

$$S(t) = \frac{\partial x}{\partial p}(t, p_0) = \begin{bmatrix} \frac{\partial x_1}{\partial p_1}(t, p_0) & \dots & \frac{\partial x_1}{\partial p_m}(t, p_0) \\ \vdots & \vdots & \vdots \\ \frac{\partial x_n}{\partial p_1}(t, p_0) & \dots & \frac{\partial x_n}{\partial p_m}(t, p_0) \end{bmatrix}, \tag{2}$$

where $S : T \to \mathbb{R}^{n \times m}$. Each entry of $S(t)$ is the derivative of a state solution with respect to a parameter, so can answer questions regarding parametric influence.

Given a model of smooth ODEs, we can solve for the sensitivity functions in equation (2) by calculating the sensitivity ODEs. For the ODE system in equation (1), the sensitivity ODEs are calculated by,

$$\begin{aligned} \dot{S}(t) &= J_p f(p_0, x(t, p_0)) + J_x f(p_0, x(t, p_0)) S(t), \\ S(t_0) &= J f(p_0), \end{aligned} \tag{3}$$

where Jf represents the Jacobian of f and $J_p f$ and $J_x f$ denote the partial Jacobian of f with respect to p and x, respectively, with IC, $S(t_0)$, and solution, $S(t)$, defined in equation (2). Therefore, solving the sensitivity ODE system in equation (3) allows one to draw conclusions on the parametric influence of the state variables, which can provide answers to questions about the sensitivity of the model.

To analyze the long-term behavior of the solutions of an ODE system, a stability analysis can be performed. This entails the calculation of the invariant sets of the model, such as the equilibria and periodic solutions, and determining the behavior of nearby solutions in the long-term. An equilibrium is a constant solution of the ODE and indicates the point at which there is no change in state variable activity. Such points

occur when the right-hand side function of the ODE system is equal to zero. Thus, an equilibrium, $x^* = (x_1^*, ..., x_n^*)$, must satisfy,

$$f(p, x^*) = 0. \tag{4}$$

A limit cycle is defined to be an isolated periodic solution, which implies it is a closed trajectory of the model, so initial conditions that lie anywhere on this solution will loop around the solution as time moves forward. The stability of an invariant set tells us how nearby trajectories (solutions) of the model behave. There are three major classifications of stability: stable, asymptotically stable, and unstable. An invariant set is stable if, for all time, nearby solutions remain nearby, but is asymptotically stable if nearby solutions approach the set as time moves forward (thus the set is “attracting" nearby solutions). In contrast, an invariant set is unstable if nearby solutions move away as time moves forward, indicating the set is “repelling" nearby solutions.

In particular, an equilibrium point, x^*, is stable if for all $\varepsilon > 0$, there exists a $\delta > 0$ such that $||x_0 - x^*|| < \delta$ implies $||x(t) - x^*|| < \varepsilon$ for a nearby solution with IC x_0. In other words, if a nearby solution is initialized within δ of a stable equilibrium point, then the solution remains within ε of the equilibrium point for all time, t. An equilibrium point, x^*, is asymptotically stable if $\lim_{t\to\infty} x(t) = x^*$ in addition to the above conditions. In terms of this definition, an equilibrium is unstable if it is not stable.

A model can have multiple equilibria. For example the ODE

$$\dot{x} = x^2 - 2x + 2 = (x-1)(x-2)$$

has an equilibrium at $x = 1$ and at $x = 2$, since both of these values result in $\dot{x} = 0$. To determine the stability of an equilibrium for a smooth ODE system, one can analyze the eigenvalues of the Jacobian matrix of the right-hand side functions of the ODEs in equation (1) with respect to x, evaluated at the equilibrium point x^*. That is, the Jacobian matrix is calculated by,

$$J_x f(p,x^*) = \begin{bmatrix} \frac{\partial f_1}{\partial x_1}(p,x^*) & \frac{\partial f_1}{\partial x_2}(p,x^*) & \dots & \frac{\partial f_1}{\partial x_n}(p,x^*) \\ \frac{\partial f_2}{\partial x_1}(p,x^*) & \frac{\partial f_2}{\partial x_2}(p,x^*) & \dots & \frac{\partial f_2}{\partial x_n}(p,x^*) \\ \vdots & \vdots & \ddots & \vdots \\ \frac{\partial f_n}{\partial x_1}(p,x^*) & \frac{\partial f_n}{\partial x_2}(p,x^*) & \dots & \frac{\partial f_n}{\partial x_n}(p,x^*) \end{bmatrix}. \tag{5}$$

The eigenvalues of the Jacobian matrix above can be used to determined the stability of the equilibrium, x^* [20]. Such eigenvalues can be found using linear algebra.

Here, let

$$J_x f(p,x^*) = \begin{bmatrix} j_{11} & j_{12} & \cdots & j_{1n} \\ j_{21} & j_{22} & \cdots & j_{2n} \\ \vdots & \vdots & \ddots & \vdots \\ j_{n1} & j_{n2} & \cdots & j_{nn} \end{bmatrix}.$$

Then the eigenvalues, λ, of the Jacobian matrix satisfies,

$$0 = \det(J_x f(p,x^*) - \lambda I_{n\times n}) = \det\left(\begin{bmatrix} j_{11}-\lambda & j_{12} & \dots & j_{1n} \\ j_{21} & j_{22}-\lambda & \dots & j_{2n} \\ \vdots & \vdots & \ddots & \vdots \\ j_{n1} & j_{n2} & \dots & j_{nn}-\lambda \end{bmatrix}\right), \tag{6}$$

where $\det(M)$ represents the determinant of the matrix M and $I_{n\times n}$ is the $n\times n$ identity matrix. Thus each eigenvalue is found by solving equation (6) for λ, which is called the characteristic equation (note that if M is a diagonal matrix, the eigenvalues are on the diagonal).

The stability of the equilibrium, x^*, can be determined by its corresponding eigenvalues. Locally, an equilibrium is asymptotically stable if the real parts of all corresponding eigenvalues are negative (i.e. for $\lambda = a+bi$, $a<0$), but if at least one eigenvalue has a positive real part (i.e. $a>0$ for at least one λ) then the equilibrium is unstable. Note that if the real part of an eigenvalue is zero (i.e. $a=0$), this test fails. Making conclusions on the stability of the equilibria of a model allows one to answer questions about the long-term behavior of the states.

The theory discussed thus far is dependent on the right-hand side functions of the ODEs involved in the model being smooth. However, some ODEs are "nonsmooth", which indicates they are nondifferentiable on some subset of their domain, therefore standard ODE analysis theories fail. Next, we will discuss theories of nonsmooth analysis that allow us to draw some conclusions on the dynamics of nonsmooth ODE models.

Generalized Derivatives

The following is adapted from concepts discussed throughout [4]. In contrast to a function being smooth (or C^1), a function $f : D_x \subseteq \mathbb{R}^n \to \mathbb{R}^m$ for $f(x) = (f_1, f_2, ..., f_m)$ and $x = (x_1, x_2, ..., x_n) \in D_x$ where D_x is an open set, can be "nonsmooth", which is continuous but indicates there is some subset $Z_f \subset D_x$ of its domain such that the function is nondifferentiable on Z_f. There are many forms of nonsmooth functions, such as piece-

wise differentiable (PC^1) functions. A function, $f(x)$, is PC^1 [21] at $x \in D_x$ if there exists a neighborhood $N \subseteq D_x$ of x and a finite collection of C^1 functions on N denoted $\mathscr{F}_f = \{f_{(1)}, ..., f_{(k)}\}$ for some positive integer k, such that f is continuous on N and the following condition is met:

$$f(y) \in \{f_{(1)}(y), \ldots, f_{(k)}(y)\}, \forall y \in N. \tag{7}$$

A function is PC^1 on the entire set D_x when f is PC^1 for each $x \in D_x$.

For example, $f(x) = |x|$ is a nonsmooth PC^1 function, since it can be broken into two C^1 functions, $f_{(1)} = x$ and $f_{(2)} = -x$, in the neighborhood of $N = \mathbb{R}$ (i.e. $\mathscr{F} = \{x, -x\}$) and every point $y \in N$ satisfies equation (7) since for $y \geq 0$, $f(y) = f_{(1)}(y)$ and for $y \leq 0$, $f(y) = f_{(2)}(y)$. Additionally, f is nonsmooth since it is nondifferentiable at the point $x = 0$. This is made clear by calculating the limit of $f'(x)$ as x approaches zero from the right (denoted with a $+$) and from the left (denoted with a $-$). Then we have,

$$\lim_{x \to 0^+} f'(x) = 1 \quad \text{and} \quad \lim_{x \to 0^-} f'(x) = -1.$$

Therefore, the limit from the right is not equal to the limit from the left, so $f(x) = |x|$ is nondifferentiable at the point $x = 0$. This implies that $Z_f = \{0\}$, confirming the fact that the function is nonsmooth.

In order to analyze the derivative information of nonsmooth functions, a theory of "generalized derivatives" has been created. There is only one stipulation of the theory, which is the need for a function to be locally Lipschitz continuous. Here, note that PC^1

functions are Lipschitz continuous, but not all Lipschitz continuous functions are PC^1. For example, $f(x) = \sqrt{x_1^2 + \cdots + x_n^2}$ is locally Lipschitz continuous but not PC^1.

A function f is Lipschitz continuous on the region $Y \subseteq D_x$ if there exists some $L > 0$ such that

$$||f(x) - f(y)|| \leq L||x - y||, \tag{8}$$

for all $x, y \in Y$. If there exists a neighborhood $N \subseteq D_x$ of x for each $x \in D_x$ so that f is Lipschitz continuous on N, then the function is locally Lipschitz continuous on D_x. If f is C^1 on D_x, then it is automatically locally Lipschitz continuous on D_x. Here, note that not all continuous functions are locally Lipschitz continuous. For example, $f(x) = \sqrt{|x|}$ is continuous, but not locally Lipschitz continuous.

Moving forward with the theory of generalized derivatives, the Bouligand subdifferential (B-subdifferential) of a locally Lipschitz continuous function f that is differentiable on the set $D_x \backslash Z_f$ for $Z_f \subset D_x$ is defined by,

$$\begin{aligned} \partial_B f(x) = \{H \in \mathbb{R}^{m \times n} : \lim_{i \to \infty} Jf(x_i) = H \text{ for some sequence } x_{(i)} \\ \text{such that } \lim_{i \to \infty} x_{(i)} = x, x_i \in D_x \backslash Z_f, \forall i \in \mathbb{N}\}. \end{aligned} \tag{9}$$

A domain (or set) $D \subseteq \mathbb{R}^n$ is convex if for every $x, y \in D$,

$$\lambda x + (1 - \lambda) y \in D \quad \forall \lambda \in [0, 1].$$

If D is a finite nonconvex set, then the convex hull of D is

$$\text{conv}(D) = \left\{ \sum_{i=1}^{m} \lambda_i x_i : m \in \mathbb{N}, \sum_{i=1}^{m} \lambda_i = 1, x_i \in D, \lambda_i \geq 0, \forall i = 1,2,...,m \right\},$$

and if D is an infinite nonconvex set, then the convex hull would be the smallest convex set D^* such that $D \subseteq D^*$. Applying the definitions above, the Clarke generalized derivative (or the Clarke Jacobian) of f, $\partial f(x)$, is the convex hull of the B-subdifferential. Thus it is calculated by,

$$\partial f(x) = \text{conv}(\partial_B f(x)), \tag{10}$$

indicating it is the convex hull of the collection of derivatives around the point x.

Returning to the example of $f(x) = |x|$, the set of nonsoothness (nondifferentiable points) is $Z_f = \{0\}$. Thus, we are interested in calculating the B-subdifferential at the point $x = 0$ in order to understand what is going on at the points of nonsmoothness. The Jacobian of $f(x)$ when x and f are a scalar is the derivative of f with respect to x (a 1×1 matrix), therefore the B-subdifferential of the absolute value of x is the set of the nearby derivatives of f. In this case, there are only two derivatives near the point $x = 0$. As calculated previously, the limit of the derivative of the absolute function of the points to the left of $x = 0$ is -1, while the limit of the points to the right is 1. Therefore,

$$\partial_B f(0) = \{-1, 1\}.$$

As stated above, the Clarke Jacobian of a function is the convex hull of the B-subdifferential,

so

$$\partial f(x) = \text{conv}\partial_B f(x) = \text{conv}\{-1,1\} = [-1,1].$$

Since this set is only two points, the convex hull is the line of points between the two values. Therefore, the Clarke Jacobian of the absolute value of x is the interval $[-1,1]$.

Clarke generalized derivatives are a useful way of differentiating nonsmooth functions since they take into account all nearby derivative information. However, they do not satisfy all standard calculus rules. For example, let $f(x) = g(x) + h(x) = \text{mid}(0,x,1) + \text{mid}(0,1-x,1)$, where $\text{mid}(a(x),b(x),c(x))$ denotes the function that compares each input, and returns the one that lies in the middle of the three (i.e. the median input) for a given value of x. Thus, when $x \leq 0$, $f(x) = 0+1 = 1$ and when $0 \leq x \leq 1$, $f(x) = x+1-x = 1$ and when $x \geq 0$, $f(x) = 1+0 = 1$ (see Figure 1). In this way, $f(x) = 1$.

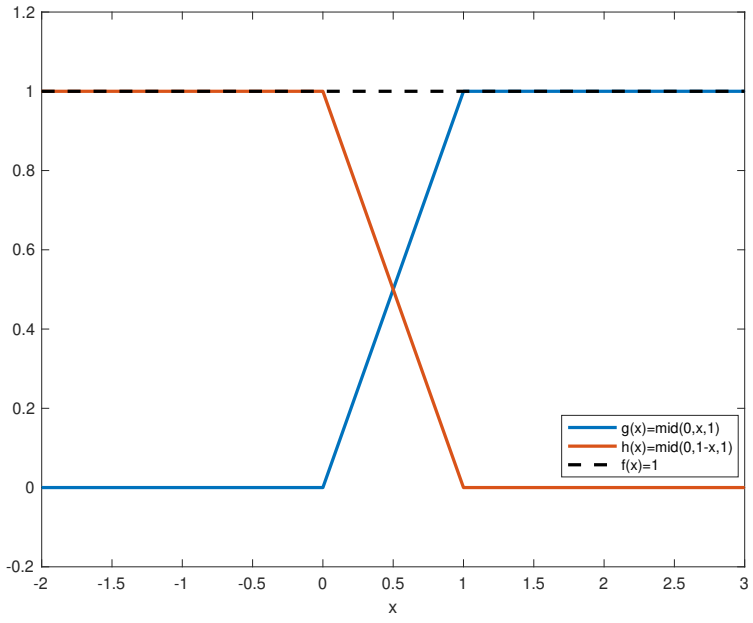

Figure 1: Mid function example.

Given the structure of $f(x)$, we would like to think that the Clarke Jacobian of $f(x)$ would be equal to the sum of the Clarke Jacobians of $g(x)$ and $h(x)$. However, the B-subdifferential of $f(x)$ at the point $x=0$ is the set $\{0\}$, so the convex hull is again the set $\{0\}$. On the other hand, the B-subdifferential of $\text{mid}(0,x,1)$ at $x=0$ is the set $\{0,1\}$, thus the Clarke Jacobian is the interval $[0,1]$ and the B-subdifferential of $\text{mid}(0,1-x,1)$ at $x=0$ is the set $\{-1,0\}$, thus the Clarke Jacobian is the interval $[-1,0]$. This implies that the sum of the Clarke Jacobians of these two mid functions is the interval $[-1,1]$. Therefore the Clarke Jacobian of $f(x)=\text{mid}(0,x,1)+\text{mid}(0,1-x,1)$ is not equal to the sum of the Clarke Jacobians of each mid function. Thus, the Clarke Jacobian does not satisfy all sharp calculus rules, such as the sum rule. For this reason, it is generally difficult to calculate Clarke generalized derivatives.

Lexicographic Differentiation

Given the Clarke generalized derivative is difficult to calculate for complex nonsmooth functions, other tools have been studied such as lexicographic differentiation [16] which does follow sharp calculus rules and is constructed from directional derivatives. The one-sided directional derivative of the function $f : X \subseteq \mathbb{R}^n \to \mathbb{R}^m$ at the point $x \in X$ and in the direction $d \in \mathbb{R}^n$ is calculated by

$$f'(x;d) = \lim_{\alpha \downarrow 0} \frac{f(x+\alpha d) - f(x)}{\alpha}. \tag{11}$$

where $\alpha \downarrow 0$ denotes that α approaches 0 from the positive side. If $f'(x;d)$ exists for all $d \in \mathbb{R}^n$, then f is directionally differentiable at x and if f is a C^1 function then

$$f'(x;d) = Jf(x)d. \tag{12}$$

The definition of a lexicographically smooth (L-smooth) [16] function is a locally Liptschitz continuous function $f : D_x \subseteq \mathbb{R}^n \to \mathbb{R}^m$ such that the following sequence of maps exists:

$$\begin{aligned}
&f_{x,P}^{(0)} : \mathbb{R}^n \to \mathbb{R}^m : d \mapsto f'(x;d), \\
&f_{x,P}^{(1)} : \mathbb{R}^n \to \mathbb{R}^m : d \mapsto [f_{x,P}^{(0)}]'(p_{(1)};d), \\
&f_{x,P}^{(2)} : \mathbb{R}^n \to \mathbb{R}^m : d \mapsto [f_{x,P}^{(1)}]'(p_{(2)};d), \\
&\quad \vdots \\
&f_{x,P}^{(k)} : \mathbb{R}^n \to \mathbb{R}^m : d \mapsto [f_{x,P}^{(k-1)}]'(p_{(k)};d),
\end{aligned} \tag{13}$$

where k is any positive integer and $P = \begin{bmatrix} p_{(1)} & \dots & p_{(k)} \end{bmatrix} \in \mathbb{R}^{n \times k}$, is called the directions matrix. If the function f is L-smooth at every point $x \in D_x$, then f is L-smooth on D_x.

The set of mappings in equation (13) is known as the homogenization sequence and involves calculations of directional derivatives as defined in equation (11). The first map of this sequence sends the direction, d, to the directional derivative of the function f. From there, the i'th map sends d to the directional derivative of the directional derivative found in the previous map (the $i-1$ map) for $i = 1,\dots,k$. The matrix P is known as the directions matrix and is built based on the directions around the point x in which derivative information is desired. Often, $P = I_{n \times n}$, but it is not required.

The homogenization sequence can be used to calculate lexicographic derivatives. When $P \in \mathbb{R}^{n\times k}$ is full row rank $\left(\text{i.e. span}\{p_{(1)},...,p_{(k)}\} = \mathbb{R}^n\right)$ and f is L-smooth at $x \in D_x$, then the final mapping $f_{x,P}^{(k)}$ in equation (13) is linear and so the lexicographic derivative (L-derivative) [16] of f is defined by,

$$J_L f(x;P) = J f_{x,P}^{(k)}(0) \in \mathbb{R}^{n\times k}. \tag{14}$$

Similarly to the B-subdifferential in equation (9), the lexicographic subdifferential (L-subdifferential), denoted $\partial_L f(x)$, is the set of L-derivatives for all direction matrices P with full row rank. Therefore,

$$\partial_L f(x) = \{J_L f(x;P) : \ \ P \in \mathbb{R}^{m\times k},\ P \text{ full row rank}\}. \tag{15}$$

The aim of this theory was to build a nonsmooth derivative that acts like the standard derivative. Using lexicographic differentiation, the nonsmooth equivalent of the classic directional derivative is known as the lexicographic directional derivative (LD-derivative) [12]. For an L-smooth function $f : D_x \subseteq \mathbb{R}^n \to \mathbb{R}^m$, the LD-derivative of f at $x \in D_x$ is calculated by,

$$f'(x;P) = \left[f_{x,P}^{(0)}(p_{(1)}) \quad f_{x,P}^{(1)}(p_{(2)}) \quad \dots \quad f_{x,P}^{(k-1)}(p_{(k)}) \right] \in \mathbb{R}^{m\times k}, \tag{16}$$

for the directional derivatives $f_{x,P}^{(i)}$ as found in the sequence in equation (13).

As proved in [12], the LD-derivative satisfies desirable calculus properties, such as the chain rule, the product rule, and more. For $f = (f_1, f_2, ..., f_n)$ and $g = (g_1, g_2, ..., g_n)$

L-smooth functions, these rules are calculated as follows:

- If $k = 1$, then $f'(x,P) = f'(x;p_{(1)})$ (i.e. when the P has one column, the LD-derivative is the directional derivative)
- If P is full row rank, then $f'(x;P) = J_L f(x;P)P$
- If f is C^1 at x, then $f'(x;P) = Jf(x)P$
- $f'(x;P) = (f_1'(x;P),...,f_n'(x;P))$
- (Sum Rule) $[f+g]'(x;P) = f'(x;P) + g'(x;P)$
- (Product Rule) $[fg]'(x;P) = g(x)f'(x;P) + f(x)g'(x;P)$ for $n = 1$
- (Chain Rule) $[f \circ g]'(x;P) = f'(g(x);g'(x;P))$

Lexicographic ordering is defined to be the generalized inequalities $\prec$ and $\preceq$ such that

$$\eta \prec \gamma \text{ if and only if } \exists j \in \{1,...,q\} \text{ such that } \eta_i = \gamma_i, \forall i < j \text{ and } \eta_i < \gamma_j,$$

$$\eta \preceq \gamma \text{ if and only if } \eta = \gamma \text{ or } \eta \prec \gamma,$$

and $\succ$ and $\succeq$ are similarly defined. A basic explanation of this ordering technique is to compare the first entries of each input and determine which is less than or greater than the other and if there is a tie (i.e. the first entries are equal), then move on to the second entries and determine which is less than or greater than the other. Carrying on in this way, once there is no longer a tie, you can determine which input is lexicographically greater or less than the other.

Returning to LD-derivative theory, once again consider the function $f(x) = |x| =$ abs(x). Then it can be shown that the LD-derivative of f for a directions matrix $m \in \mathbb{R}^{1\times k}$ is calculated by,

$$\text{abs}'(x;m) = \text{fsign}(x, m^T)m,$$

where fsign(x) is the "first-sign function" such that

$$\text{fsign}(x, m^T) = \begin{cases} 1, & \text{if } (x, m^T) \succ \mathbf{0}_{(k+1)\times 1}, \\ -1, & \text{if } (x, m^T) \prec \mathbf{0}_{(k+1)\times 1}, \\ 0, & \text{if } (x, m^T) = \mathbf{0}_{(k+1)\times 1}, \end{cases}$$

where $\mathbf{0}_{i\times j}$ denotes the $i \times j$ zero matrix.

As another example, we will investigate the LD-derivative of the mid function, as it will be used throughout this thesis. As explained above, the mid function inputs three functions, $f(x,y,z)$, $g(x,y,z)$, and $h(x,y,z)$, and returns the median input. The “lexicographic mid" (lmid) function uses lexicographic ordering to determine the entry that lies in the middle of the others (i.e. the median input). Therefore, lmid$(x,y,z) = y$ if $x \preceq y \preceq z$. For example,

$$\text{lmid}\left(\begin{bmatrix}1 & 2 & 3\end{bmatrix}, \begin{bmatrix}1 & 4 & 7\end{bmatrix}, \begin{bmatrix}1 & 4 & 9\end{bmatrix}\right) = \begin{bmatrix}1 & 4 & 7\end{bmatrix}.$$

Since the first entries of all three inputs are equal, we must move on and compare the second entries. However, there is a tie here as well, thus we must move to the third entries, from which we can conclude that the second input is the median of the three.

By the above theory, it can be shown that the LD-derivative of the mid function is

$$[\text{mid}\circ(f,g,h)]'(x,y,z;(X,Y,Z)) = \text{slmid}\Big(\begin{bmatrix} f & J_x f X + J_y f Y + J_z f Z \end{bmatrix}, \begin{bmatrix} g & J_x g X + J_y g Y + J_z g Z \end{bmatrix}, \begin{bmatrix} h & J_x h X + J_y h Y + J_z h Z \end{bmatrix}\Big), \tag{17}$$

for directions matrix $P = (X,Y,Z)$, where the functions above are evaluated at (x,y,z). Here, slmid refers to the “shifted-lexicographic" mid function, which, similarly to the lmid function, lexicographically compares the three input vectors and outputs the median input but without the left-most entry. In comparison to the lmid example above, the slmid function follows the below calculation:

$$\text{slmid}\Big(\begin{bmatrix}1 & 2 & 3\end{bmatrix},\begin{bmatrix}1 & 4 & 7\end{bmatrix},\begin{bmatrix}1 & 4 & 9\end{bmatrix}\Big) = \begin{bmatrix}4 & 7\end{bmatrix},$$

since the output vector is the median input, however the left-most entry, 1, is no longer included.

Since these derivatives follow sharp calculus rules, lexicographic differentiation is a key tool to analyzing nonsmooth ODE systems. As explained previously, understanding the dynamics of a nonsmooth model can be done by methods that involve investigating the derivatives of the system. Lexicographic differentiation provides a way to do this even if the model is nonsmooth, allowing for the nonsmooth analysis performed throughout this thesis.

Applying the theories of generalized derivatives and lexicographic differentiation has allowed for the analysis of the dynamics of nonsmooth systems by replacing standard derivatives with generalized derivatives. For the ODE model with state variables $x = (x_1,...,x_n)$ and parameters $p = (p_1,...,p_m)$ in equation (1), but now with L-smooth right-hand side functions f and f_0, the L-sensitivity functions are calculated by [11],

$$S(t) = J_L[x(t,\cdot)](p_0;P) = \begin{bmatrix} J_L[x_1(t,\cdot)](p_0;P) \\ \vdots \\ J_L[x_n(t,\cdot)](p_0;P) \end{bmatrix}, \tag{18}$$

which is equivalent to the smooth sensitivity functions in equation (2).

The L-sensitivity functions can be found using the solutions to the nonsmooth sensitivity ODEs, which are obtained by taking the LD-derivatives of the model ODEs. Thus the sensitivity ODEs are calculated by [11],

$$\begin{aligned} \dot{X}(t) &= f'(p_0, x(t,p_0); (P, X(t))), \\ X(t_0) &= f_0'(p_0;P), \end{aligned} \tag{19}$$

for the initial condition $X(t_0)$ and directions matrix P. The term $X(t)$ represents the solution of the nonsmooth sensitivity system, which allows us to recover the nonsmooth L-sensitivity function, $S(t)$.

As stated previously, there is a relationship between the LD-derivative of a function and the L-derivative. If the L-derivative is known and the directions matrix is full

row rank, the LD-derivative, $X(t)$, can be calculated by,

$$X(t) = S(t)P,$$

for the directions matrix P. This relationship implies,

$$S(t) = X(t)P^{-1}, \tag{20}$$

where P^{-1} is the right-inverse matrix of P (which is the inverse of P when P is square and nonsingular). Therefore, if the LD-derivative is known, we can use the above relationship to solve for the L-derivative. In terms of a nonsmooth sensitivity analysis, equation (20) shows that the L-sensitivity function, $S(t)$, of a nonsmooth ODE system is derived from the solution, $X(t)$, to the sensitivity ODEs of the model.

Now we want to show that if the right-hand-side functions of the model ODEs are smooth and $P = I$ (for the identity matrix I), then we recover the smooth sensitivity ODEs of equation (3) from the nonsmooth sensitivity ODEs. As stated in the previous subsection, LD-derivatives satisfy the property, $f'(x;P) = Jf(x)P$, when f is C^1 at x. Therefore the nonsmooth sensitivity ODE system for C^1 functions f and f_0 and direc-

tions matrix $P = I$ is,

$$\begin{aligned}
\dot{X}(t) &= f'(p_0, x(t,p_0); (P, X(t))) \\
&= Jf(x)(I, X(t)) = \begin{bmatrix} J_p f(p_0, x(t,p_0)) & J_x f(p_0, x(t,p_0)) \end{bmatrix} \begin{bmatrix} I \\ X(t) \end{bmatrix} \qquad (21) \\
&= J_p f(p_0, x(t,p_0)) + J_x f(p_0, x(t,p_0)) X(t), \\
X(t_0) &= f_0'(p_0; P) = Jf_0(p_0) I = Jf_0(p_0),
\end{aligned}$$

for initial condition $X(t_0)$. The sensitivity equations in equation (21) exactly match the sensitivity ODEs in equation (3). Therefore a nonsmooth sensitivity analysis of a smooth ODE system recovers the smooth sensitivity analysis.

In comparison to a stability analysis of a smooth ODE model, the stability of a nonsmooth model can be difficult to determine. If an equilibrium lies on a region of nonsmoothness, linearization of the system fails, since the Jacobian of an ODE model is based on derivative information. There are other techniques that can be applied to nonsmooth models, such as Lyapunov functions [24], although it is generally difficult to come up with a function to apply to your chosen model. Having said that, since a nonsmooth model is differentiable almost everywhere, equilibria could lie in parts of the model that are smooth. In these cases, one can linearize the model via the Jacobian matrix and analyze its eigenvalues. This happens to be the case for the nonsmooth model studied in this thesis, therefore the nonsmooth stability analysis performed in this project was completed using smooth methods.

CHAPTER III

MODEL FORMULATION

Wilson-Cowan Type Neural Mass Models

The Wilson-Cowan neural mass model [28] is a popular mathematical model that groups excitatory and inhibitory neural populations and models their communication [5]. For a background in mathematical neural mass models, the reader may refer to [7, 27]. In the Wilson-Cowan model, a population of excitatory neurons is coupled to a population of inhibitory neurons through the transfer of neural signals between one another and the relationship of the two groups can be modeled by equations representing the firing rate of neurons at a given time in each population. The so-called minimal model, implying it models two isolated neural populations, is given by the following ODEs:

$$\begin{aligned} \dot{u} &= -u + F(I_u + w_{uu}u - w_{vu}v), \qquad u(0) = u_0, \\ \dot{v} &= \frac{1}{\tau}[-v + F(I_v + w_{uv}u - w_{vv}v)], \qquad v(0) = v_0, \end{aligned} \tag{22}$$

where $p = (\tau, \varepsilon, I_u, I_v, w_{uu}, w_{vu}, w_{uv}, w_{vv}, u_0, v_0)$ is a vector of problem parameters (see Table 1). The state variables of the model are u and v, which indicate the proportion of excitatory cells firing per unit time and the proportion of inhibitory cells firing per unit time, respectively. This implies the ODEs in equation (22) represent the change in firing rate within each population, rather than the change in individual spikes. This choice

was made since the dynamics of neuron firing rates have been studied more frequently and therefore have many more biological applications than the dynamics of individual spikes [7]. Since the state variables represent a proportion of the population firing per unit time, they take on values between zero and one, where zero is equivalent to 0% of the given population firing and one is equivalent to 100% of the given population firing. The function $F(x)$ is the firing rate function of the model, which represents the proportion of neurons receiving at least threshold excitation in a given population and can take on different functional forms. The proportion of firing neurons depends on the firing rates of both populations, therefore $F(x)$ is dependent on both state variables of the model.

Model Parameters		
p_i	*Description*	p_i^0
τ	relative time scale	0.6
ε	sharpness factor of firing rate funtion	100
I_u	external inputs to u population	-0.05
I_v	external inputs to v population	-.3
w_{uu}	weight of synapses from u population to u population	1
w_{vu}	weight of synapses from v population to u population	2
w_{uv}	weight of synapses from u population v population	1
w_{vv}	weight of synapses from v population to v population	0.25
u_0	initial value of firing excitatory neurons	0.32
v_0	initial value of firing excitatory neurons	0.14

Table 1: Parameters in equation (22), with reference values from [5].

The ODEs in equation (22) capture the relationship between a population of excitatory neurons and a population of inhibitory neurons as they communicate with

each other through neural signals (action potentials), which are passed by the presynaptic neuron to the postsynaptic neuron. The signal of an excitatory neuron causes the postsynaptic neuron to fire, so an increase in the firing rate of an excitatory neuron will increase the proportion of neurons firing, implying excitatory inputs involved in the firing rate function must be represented by positive terms in both ODE equations [27]. In contrast to excitatory neurons, the signal of an inhibitory neuron prevents the firing of an action potential in the postsynaptic neuron, so an increase in the firing of inhibitory neurons results in a decrease in the proportion of neurons firing. Thus, inhibitory signals should be represented by negative terms in the model equations. The terms $-u$ and $-v$ represent the leak terms from the excitatory population and inhibitory population, respectively, and quantify the number of neurons firing to neurons outside the two considered populations per unit time, therefore exiting the group of isolated populations being considered in this model [9].

The parameters of the ODE equations in equation (22) determine the dynamics of the Wilson-Cowan model. The ODE equation representing the change in the number of inhibitory neurons firing, $\dot{v}$, is scaled by the time constant parameter, τ, because inhibitory neurons tend to fire at a quicker rate than excitatory neurons [25]. Since it represents a faster timescale, we assume this parameter to be less than one (i.e. $\tau < 1$). Another parameter of the Wilson-Cowan model is the sharpness factor of the firing rate function, ε, which determines the gain (or slope) of the firing rate function, $F(x)$.

The parameters w_{ij}, for $i, j \in \{u, v\}$, represent the connection strength, or weight, between neurons in the i population communicating with the j population. A stronger connection between two populations implies an action potential can be transferred

more quickly, therefore the rate of firing is greater than the rate between neurons with a weaker connection. Here, the model assumes that any connection between two kinds of neurons is equal no matter which two are being considered, which is why all excitatory neurons can be grouped into one population and the same can be done for all inhibitory neurons. This implies that the weight between any two excitatory neurons is equivalent to the weight between any other two excitatory neurons, the weight between any two inhibitory neurons is equivalent to the weight between any other two inhibitory neurons, and the weight between any excitatory and any inhibitory neuron is equivalent to the weight between any other excitatory and inhibitory neuron (or vice versa).

Other parameters are I_i, which are the external inputs to the i population (for $i, j \in \{u, v\}$), which represent any signals coming from neurons outside the u or v populations. As discussed in Chapter II, the Wilson-Cowan model can be applied to neural networks of many brain regions, thus outside inputs can come from neurons located in other brain areas not considered in the Wilson-Cowan model. For example, if the model were applied to a neural network of the visual cortex, outside inputs might be coming from neurons located in the thalamus. The final parameters of the model are the initial conditions, u_0 and v_0, of the state variables, which represent the proportion of firing neurons in each population at the initial time, t_0. As described above, the states take on values between zero and one, thus $(u_0, v_0) \in [0,1]^2$.

Firing Rate Function Choices

In the literature, the firing rate function $F(x)$ is typically modeled by a smooth sigmoid curve such as,

$$F(x) = \text{expit}(x) = \frac{1}{1+e^{-\varepsilon x}}. \tag{23}$$

We will denote the Smooth Wilson-Cowan model as the model involving this firing rate function. By construction, increasing the sharpness factor, ε, in equation (23) will increase the gain of expit(x), as shown in Figure 2. However, the smooth form of the firing rate function may not have been biologically motivated in its creation [3], thus other forms firing rate functions have been studied.

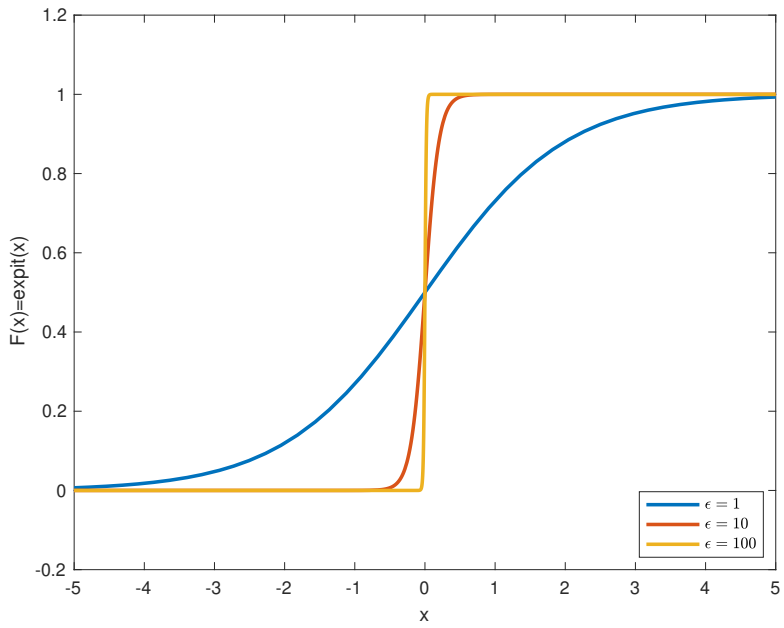

Figure 2: Smooth firing rate function with $F(x)$ in equation (23) for various sharpness factors, ε.

A nonsmooth firing rate function, $F(x)$, can also be used in the Wilson-Cowan Model, such as the piecewise-linear (PWL) function analyzed in [5]. This function can

be represented by the following mid function,

$$F(x) = \text{mid}(0, \varepsilon^{-1}x, 1) = \begin{cases} 0, & \text{if } x \leq 0, \\ \varepsilon^{-1}x, & \text{if } 0 < x < \varepsilon, \\ 1, & \text{if } x \geq \varepsilon, \end{cases} \tag{24}$$

which is equal to zero when 0% of a given population is receiving at least threshold potential (thus all neurons are at rest), until a threshold is reached. Then there is an incline that represents the increasing proportion of firing neurons, until the firing rate function reaches one, which represents 100% of a given population firing. In contrast to the smooth firing rate function in equation (23), decreasing the sharpness factor, ε, in equation (24) will increase the gain of the PWL curve, as shown in Figure 3.

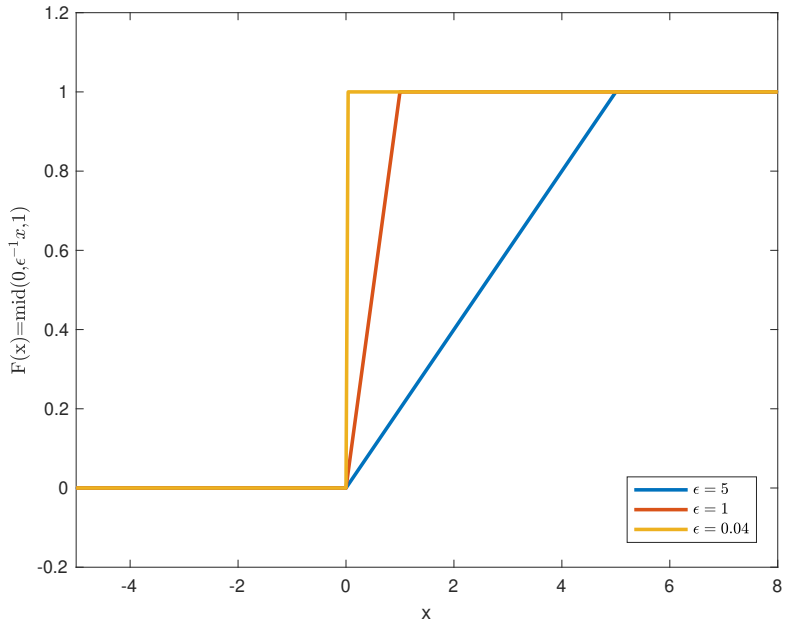

Figure 3: Nonsmooth firing rate function with $F(x)$ in equation (24) for various sharpness factors, ε.

The fact that the firing rate of equation (23) is centered at $x = 0$, while the firing rate of equation (24) is centered at $x = \frac{\varepsilon}{2}$, proves to be a limitation when comparing the models. Therefore a PWL function built based on the tangent line to the midpoint of equation (23) and centered at $x = 0$ is more favorable to the analysis we would like to carry out. Thus, we used the firing rate function

$$F(x) = \text{mid}\left(0, \frac{\varepsilon}{4}x + \frac{1}{2}, 1\right) = \begin{cases} 0, & \text{if } x \leq -\frac{2}{\varepsilon}, \\ \frac{\varepsilon}{4}x + \frac{1}{2}, & \text{if } -\frac{2}{\varepsilon} < x < \frac{2}{\varepsilon}, \\ 1, & \text{if } x \geq \frac{2}{\varepsilon}, \end{cases} \tag{25}$$

to represent what we call the Nonsmooth Wilson-Cowan model, which is made up of the ODE system in equation (22) with the above firing rate function.

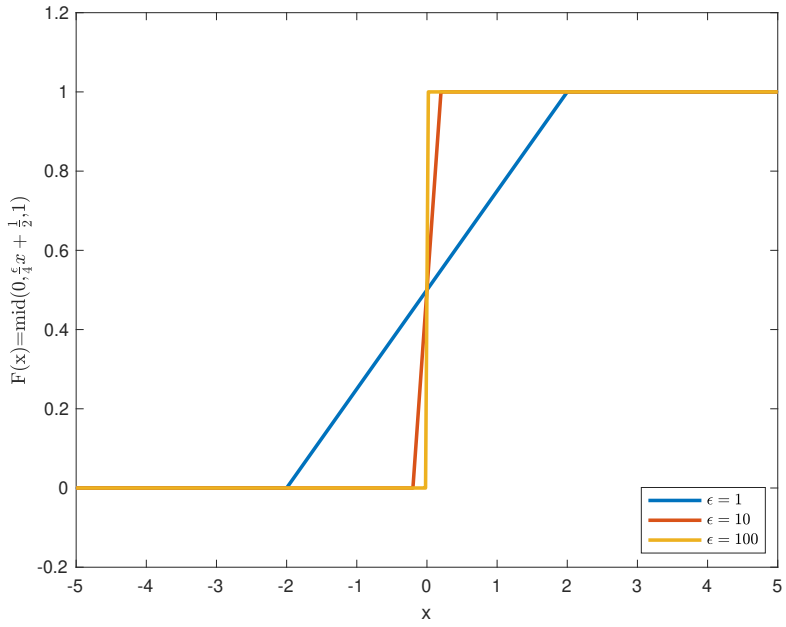

Figure 4: Nonsmooth firing rate function with $F(x)$ in equation (25) for various sharpness factors, ε.

This PWL firing rate function, identically to expit(x), is centered at $x = 0$ and increasing the sharpness factor, ε, increases the gain of equation (25), as shown by Figure 4. Moving forward, we implemented this function as it will more easily allow us to compare the results of the Smooth Wilson-Cowan model to that of the Nonsmooth Wilson-Cowan model.

Numerical Solutions of Nonsmooth Model

Simulating the ODE system in equation (22) using the nonsmooth firing rate of equation (25) allowed us to analyze the behavior of the state variables, u and v, of the model by using MATLAB to solve the ODE system for specific initial conditions, (u_0, v_0). We plotted these variables in Figure 5 vs time, t, and have included a phase portrait in Figure 6.

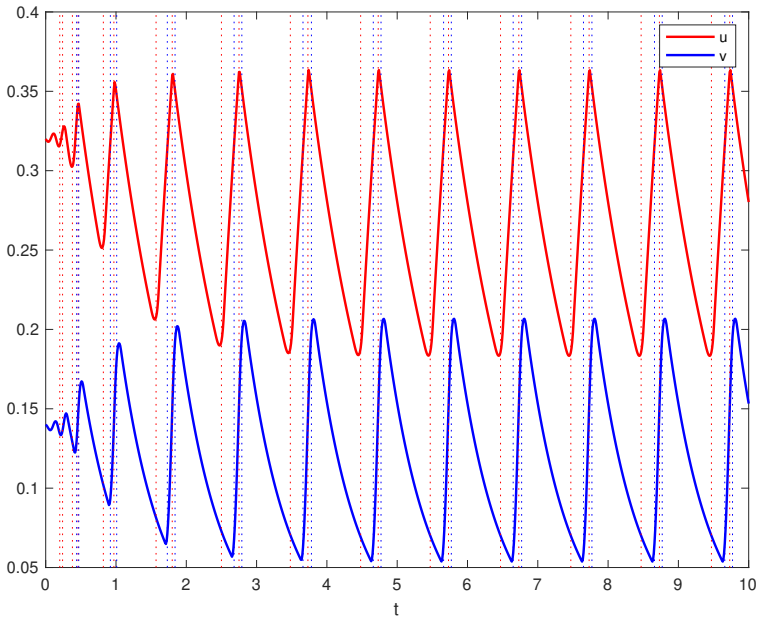

Figure 5: State variable behavior vs time with ICs $(u_0, v_0) = (0.32, 0.14)$. Red and blue vertical, dotted lines represent times when the nonsmooth F(x) in equation (4) switches outputs.

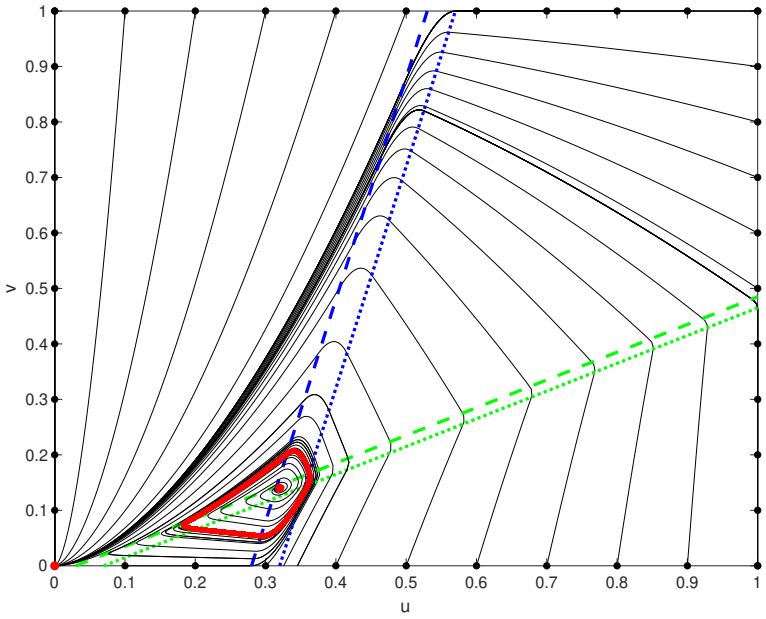

Figure 6: Phase portrait of state variable u vs state variable v for a rang of ICs. Blue and green dashed lines represent switching manifolds of the arguments in equation (4) and black dots around the perimeter represent each IC. Red solutions represent possible invariant sets.

The vertical, dotted lines in Figure 5 are the times when the nonsmooth firing rate function switches outputs, therefore these points represent the nonsmooth parts of the model. The nonsmooth firing rate function in equation (25) has three possible output arguments based on the input argument, x. Thus, when the input crosses any of the thresholds, $F(x)$ switches outputs. As shown in the above figure, there are many instances of nonsmoothness, indicating the need for the nonsmooth ODE theory described in Chapter II.

While analyzing the state variable behavior of the model, it was found that some initial conditions result in a spiking behavior of u and v, where the excitatory neuron firing rate is balanced by inhibitory neurons. Figure 5 indicates that as the firing rate of the excitatory neuron population increases, the firing rate of the inhibitory neuron

population increases which, it turn, decreases the firing rates of all neurons involved in the network. Then excitatory firing rates begin to climb again, resulting in this constant spiking behavior. From here, we would like to determine which of the 10 problem parameters listed in Table 1 influence this spiking behavior of the Nonsmooth Wilson-Cowan model the most, which will provide information about the dynamics between the two neuron populations.

CHAPTER IV

SENSITIVITY ANALYSIS

The first goal of this thesis is to determine the parameters of the model that most influence the dynamics of the state variables. In order to do this we performed a sensitivity analysis. As discussed in Chapter II, this entails calculating the sensitivity equations, which involve the derivatives of the right-hand side functions of the ODEs in the classical case. However, since we have used a nonsmooth PWL firing rate function, such equations must be computed using "generalized derivatives", which are calculated here using lexicographic differentiation.

Derivation of Nonsmooth Sensitivity Equations

Following the nonsmooth sensitivity analysis described in Chapter II, it can be shown that the sensitivity system of the nonsmooth Wilson-Cowan model is calculated by,

$$\begin{aligned} \dot{X}(t) &= f'(p_0, x(t,p_o);(P,X(t))) = \begin{bmatrix} f'_u(p_0, x(t,p_0);(P,X(t))) \\ f'_v(p_0, x(t,p_0);(P,X(t))) \end{bmatrix}, \\ X(t_0) &= f'_0(p_0;P) = \begin{bmatrix} f'_{0,u}(p_0;P) \\ f'_{0,v}(p_0;P) \end{bmatrix}, \end{aligned} \tag{26}$$

where $x(t,p_0)=(u(t,p_0),v(t,p_0))$, $f(p,x)=(f_u(p,x),f_v(p,x))$, P is a 10×10 directions matrix and X(t) is the 2×10 solutions matrix, denoted

$$X(t)=\begin{bmatrix} X_u(t) \\ \\ X_v(t) \end{bmatrix}.$$

Here, $f'(p_0,x(t,p_o);(P,X(t)))$ is the LD-derivative of the right-hand-side function of the model's ODE equations. Therefore, the sensitivity equations of the nonsmooth Wilson-Cowan model are calculated as follows:

$$\begin{aligned} \dot{X}(t) &= \begin{bmatrix} [-u+F(I_u+w_{uu}u-w_{vu}v]' \\ \\ [-v+F(I_v+w_{uv}u-w_{vv}v)]' \end{bmatrix} \\ &= \begin{bmatrix} [-u]'+[F(I_u+w_{uu}u-w_{vu}v)]' \\ \\ [\frac{-v}{\tau}]'+[\frac{1}{\tau}(F(I_v+w_{uv}u-w_{vv}v))]' \end{bmatrix} \\ &= \begin{bmatrix} [-u]' \\ \\ [\frac{-v}{\tau}]' \end{bmatrix} + \begin{bmatrix} [F(I_u+w_{uu}u-w_{vu}v)]' \\ \\ [\frac{1}{\tau}(F(I_v+w_{uv}u-w_{vv}v))]' \end{bmatrix} \end{aligned} \tag{27}$$

where $[\cdot]'$ denotes the LD-derivative of the argument evaluated at references $(p_0,x(t,p_0))$ in the directions $(P,X(t))$.

For simplicity, let

$$A=\begin{bmatrix} [-u]' \\ \\ [\frac{-v}{\tau}]' \end{bmatrix} \text{ and } B=\begin{bmatrix} [F(I_u+w_{uu}u-w_{vu}v)]' \\ \\ [\frac{1}{\tau}(F(I_v+w_{uv}u-w_{vv}v))]' \end{bmatrix}.$$

Since matrix A is made up of smooth functions, we can use equation (12) to calculate

the LD-derivatives. Thus the left matrix follows the below calculations:

$$
\begin{aligned}
A &= \begin{bmatrix} [-u]' \\ [\frac{-v}{\tau}]' \end{bmatrix} \\
&= \begin{bmatrix} J[-u](P,X(t)) \\ J[\frac{-v}{\tau}](P,X(t)) \end{bmatrix} \\
&= \begin{bmatrix} J_p[-u] \\ J_p[\frac{-v}{\tau}] \end{bmatrix} P + \begin{bmatrix} J_x[-u] \\ J_x[\frac{-v}{\tau}] \end{bmatrix} X(t) \\
&= \begin{bmatrix} 0 & \mathbf{0}_{1x9} \\ \frac{v}{\tau^2} & \mathbf{0}_{1x9} \end{bmatrix} P + \begin{bmatrix} \frac{\partial(-u)}{\partial u} & \frac{\partial(-u)}{\partial v} \\ \frac{\partial(\frac{-v}{\tau})}{\partial u} & \frac{\partial(\frac{-v}{\tau})}{\partial u} \end{bmatrix} \begin{bmatrix} X_u(t) \\ X_v(t) \end{bmatrix} \\
&= \begin{bmatrix} 0 & \mathbf{0}_{1x9} \\ \frac{v}{\tau^2} & \mathbf{0}_{1x9} \end{bmatrix} P + \begin{bmatrix} -1 & 0 \\ 0 & \frac{-1}{\tau} \end{bmatrix} \begin{bmatrix} X_u(t) \\ X_v(t) \end{bmatrix} \\
&= \begin{bmatrix} -X_u(t) \\ \left(\frac{1}{\tau}\right)\left(\begin{bmatrix} \frac{v}{\tau} & \mathbf{0}_{1x9} \end{bmatrix} P - X_v(t)\right) \end{bmatrix} \\
&= \begin{bmatrix} -X_u(t) \\ \left(\frac{1}{\tau}\right)\left(\frac{v}{\tau} P_1 - X_v(t)\right) \end{bmatrix},
\end{aligned}
$$

where P_i for $i = 1,...,10$ denotes the i'th row of P.

Now we want to calculate matrix B in equation (27). The nonsmooth firing rate function in equation (25) is a PWL function, which can be described by the mid function,

$$F(x) = \text{mid}\left(0, \frac{\varepsilon}{4}x + \frac{1}{2}, 1\right). \tag{28}$$

As outlined in Chapter II, the LD-derivative of the mid function is the slmid function (see equation (17)). Due to the length of the following equations, we have created several variables to simplify the calculations as found in Table 2. Thus, the LD-derivative of the PWL firing rate function of the nonsmooth Wilson-Cowan model with respect to state variable u is calculated by,

$$\begin{aligned}
&\left[\text{mid}\circ\left(0,\tfrac{\varepsilon}{4}x_u+\tfrac{1}{2},1\right)\right]'(p_0,x(t,p_0);(P,X(t))) \\
&\qquad = \text{slmid}\Bigg(\begin{bmatrix} 0 & J_p(0)P+J_u(0)X(t)\end{bmatrix}, \\
&\qquad\qquad \begin{bmatrix} \tfrac{\varepsilon}{4}x_u+\tfrac{1}{2} & J_p\left(\tfrac{\varepsilon}{4}x_u+\tfrac{1}{2}\right)P+J_u\left(\tfrac{\varepsilon}{4}x_u+\tfrac{1}{2}\right)X(t)\end{bmatrix}, \\
&\qquad\qquad \begin{bmatrix} 1 & J_p(1)P+J_u(1)X(t)\end{bmatrix}\Bigg) \\
&\qquad = \text{slmid}\Bigg(\begin{bmatrix} 0 & \mathbf{0}_{1x10}\end{bmatrix}, \\
&\qquad\qquad \begin{bmatrix} \tfrac{\varepsilon}{4}x_u+\tfrac{1}{2} & J_p(\tfrac{\varepsilon}{4}x+\tfrac{1}{2})P+J_u(\tfrac{\varepsilon}{4}x_u+\tfrac{1}{2})X(t)\end{bmatrix}, \\
&\qquad\qquad \begin{bmatrix} 1 & \mathbf{0}_{1x10}\end{bmatrix}\Bigg).
\end{aligned}$$

The LD-derivative of the firing rate function of the nonsmooth model with respect to the state variable v is calculated similarly.

Returning to matrix B, the nonsmooth product rule must also be used, since this matrix involves the nonsmooth firing function being multiplied by the term $\frac{1}{\tau}$. Therefore, the right matrix of the sensitivity system in equation (36) is calculated by the

Nonsmooth Sensitivity Equation Auxiliary Variables	
Symbol	Expression
x_u	$I_u + w_{uu}u - w_{vu}v$
x_v	$I_v + w_{uv}u - w_{vv}v$
F_u	$\frac{\varepsilon}{4}(x_u) + \frac{1}{2}$
F_v	$\frac{\varepsilon}{4}(x_v) + \frac{1}{2}$
mid_u	$mid(0, F_u, 1)$
mid_v	$mid(0, F_v, 1)$
F_u'	$-\frac{x_u}{\varepsilon^2}P_2 + \frac{1}{\varepsilon}P_3 + \frac{u}{\varepsilon}P_5 - \frac{v}{\varepsilon}P_6 + w_{uu}S_u - w_{vu}S_v$
F_v'	$-\frac{x_v}{\tau^2\varepsilon}P_1 - \frac{f_v}{\varepsilon^2}P_2 + \frac{1}{\varepsilon}P_4 + \frac{u}{\varepsilon}P_7 - \frac{v}{\varepsilon}P_8 + w_{uv}S_u - w_{vv}S_v$

Table 2: Variables in equation (29) that simplify the derivation of the Nonsmooth Wilson-Cowan sensitivity equations.

following:

$$
\begin{aligned}
B &= \begin{bmatrix} [F(I_u + w_{uu}u - w_{vu}v)]' \\ [\frac{1}{\tau}(F(I_v + w_{uv}u - w_{vv}v))]' \end{bmatrix} \\
&= \begin{bmatrix} [\mathrm{mid}_u]' \\ \left[\frac{1}{\tau}\right]'(\mathrm{mid}_v) + \left(\frac{1}{\tau}\right)[\mathrm{mid}_v]' \end{bmatrix} \\
&= \begin{bmatrix} \mathrm{slmid}\left(\begin{bmatrix} 0 & \mathbf{0}_{1x10} \end{bmatrix}, \begin{bmatrix} F_u & F_u' \end{bmatrix}, \begin{bmatrix} 1 & \mathbf{0}_{1x10} \end{bmatrix}\right) \\ \left(J\left[\frac{1}{\tau}\right](P, X(t))\right)(\mathrm{mid}_v) + \left(\frac{1}{\tau}\right)\mathrm{slmid}\left(\begin{bmatrix} 0 & \mathbf{0}_{1x10} \end{bmatrix}, \begin{bmatrix} F_v & F_v' \end{bmatrix}, \begin{bmatrix} 1 & \mathbf{0}_{1x10} \end{bmatrix}\right) \end{bmatrix} \\
&= \begin{bmatrix} \mathrm{slmid}\left(\begin{bmatrix} 0 & \mathbf{0}_{1x10} \end{bmatrix}, \begin{bmatrix} F_u & F_u' \end{bmatrix}, \begin{bmatrix} 1 & \mathbf{0}_{1x10} \end{bmatrix}\right) \\ \left(J_p\left[\frac{1}{\tau}\right]P + J_x\left[\frac{1}{\tau}\right]X(t)\right)(\mathrm{mid}_v) + \left(\frac{1}{\tau}\right)\mathrm{slmid}\left(\begin{bmatrix} 0 & \mathbf{0}_{1x10} \end{bmatrix}, \begin{bmatrix} F_v & F_v' \end{bmatrix}, \begin{bmatrix} 1 & \mathbf{0}_{1x10} \end{bmatrix}\right) \end{bmatrix} \\
&= \begin{bmatrix} \mathrm{slmid}\left(\begin{bmatrix} 0 & \mathbf{0}_{1x10} \end{bmatrix}, \begin{bmatrix} F_u & F_u' \end{bmatrix}, \begin{bmatrix} 1 & \mathbf{0}_{1x10} \end{bmatrix}\right) \\ \left(\begin{bmatrix} -\frac{1}{\tau^2} & \mathbf{0}_{1x9} \end{bmatrix}P\right)(\mathrm{mid}_v) + \left(\frac{1}{\tau}\right)\mathrm{slmid}\left(\begin{bmatrix} 0 & \mathbf{0}_{1x10} \end{bmatrix}, \begin{bmatrix} F_v & F_v' \end{bmatrix}, \begin{bmatrix} 1 & \mathbf{0}_{1x10} \end{bmatrix}\right) \end{bmatrix},
\end{aligned}
\tag{29}
$$

which implies,

$$B = \begin{bmatrix} \text{slmid}\left(\begin{bmatrix} 0 & \mathbf{0}_{1x10} \end{bmatrix}, \begin{bmatrix} F_u & F_u' \end{bmatrix}, \begin{bmatrix} 1 & \mathbf{0}_{1x10} \end{bmatrix}\right) \\ \left(\frac{1}{\tau}\right)\left(-\frac{1}{\tau}P_1(\text{mid}(x_v)) + \text{slmid}\left(\begin{bmatrix} 0 & \mathbf{0}_{1x10} \end{bmatrix}, \begin{bmatrix} F_v & F_v' \end{bmatrix}, \begin{bmatrix} 1 & \mathbf{0}_{1x10} \end{bmatrix}\right)\right) \end{bmatrix}. \tag{30}$$

The ICs, $X_u(t_0)$ and $X_v(t_0)$, of the sensitivity equations are the LD-derivatives of the ICs, $u(0)$ and $v(0)$, of the model ODEs in equation (22) with respect to p. Therefore,

$$X_u(t_0) = f_{0,u}'(p_0;P) = Jf_{0,u}(p_0;P)P = \begin{bmatrix} \mathbf{0}_{1\times 8} & 1 & 0 \end{bmatrix} P = P_9$$
$$X_v(t_0) = f_{0,v}'(p_0;P) = Jf_{0,v}(p_0;P)P = \begin{bmatrix} \mathbf{0}_{1\times 8} & 0 & 1 \end{bmatrix} P = P_{10}.$$

After combining all above calculations, the sensitivity equations of the nonsmooth Wilson-Cowan model are:

$$\begin{aligned} \dot{X}_u &= -X_u + \text{slmid}\left(\begin{bmatrix} 0 & \mathbf{0}_{1x10} \end{bmatrix}, \begin{bmatrix} F_u & F_u' \end{bmatrix}, \begin{bmatrix} 1 & \mathbf{0}_{1x10} \end{bmatrix}\right), \\ \dot{X}_v &= \left(\frac{1}{\tau}\right)\left(\left(\frac{v - mid(x_v)}{\tau^2}\right)P_1 - X_v + \text{slmid}\left(\begin{bmatrix} 0 & \mathbf{0}_{1x10} \end{bmatrix}, \begin{bmatrix} F_v & F_v' \end{bmatrix}, \begin{bmatrix} 1 & \mathbf{0}_{1x10} \end{bmatrix}\right)\right), \\ X_u(t_0) &= P_9, \\ X_v(t_0) &= P_{10}. \end{aligned} \tag{31}$$

The sensitivity function, $S(t)$, is then calculated by,

$$S(t) = X(t)P^{-1}. \tag{32}$$

Since there are 10 problem parameters and 2 state variables, there are a total of 20

sensitivity functions each corresponding to one parameter, p_j (for $j=1,...,10$) and one state variable x_i (for $i=1,2$ where $x_1=u$ and $x_2=v$). Therefore the nonsmooth sensitivities can be represented by the $2x10$ matrix,

$$S(t)=\begin{bmatrix} S_{x_1}^{p_1}(t) & S_{x_1}^{p_2}(t) & \dots & S_{x_1}^{p_{10}}(t) \\ S_{x_2}^{p_1}(t) & S_{x_2}^{p_2}(t) & \dots & S_{x_2}^{p_{10}}(t) \end{bmatrix}$$

where the term $S_{x_i}^{p_j}(t)$ denotes each sensitivity solution, which roughly represents the change in behavior of x_i when the parameter value p_j is varied, associated with the probing directions in P.

Local Sensitivity Analysis of Nonsmooth Model

A local sensitivity analysis is performed using a set of reference parameter values and initial conditions. For this portion of the analysis we used the parameter values found in Table 1 and simulated the sensitivity ODEs of equation (31) in order to solve for the sensitivities, $S(t)$ (note that $P=I$ was used for all sensitivity equation simulations, so $S(t)=X(t)$ in this case). The results of this simulation are shown in Figures 7 and 8.

To get a clearer picture of the sensitivity activity, we compared the behavior of each sensitivity solution, $S_{x_i}^{p_j}(t)$, to the results of the relative sensitivity solution, $\hat{S}_{x_i}^{p_j}(t)$, which are calculated by

$$\hat{S}_{x_i}^{p_j}(t)=S_{x_i}^{p_j}(t)\times\frac{p_j^0}{x_i(t,p_j^0)+1}. \tag{33}$$

The need for a relative sensitivity analysis is due to the differences in magnitudes of the parameter values and corresponding reference solutions. This is addressed by scaling

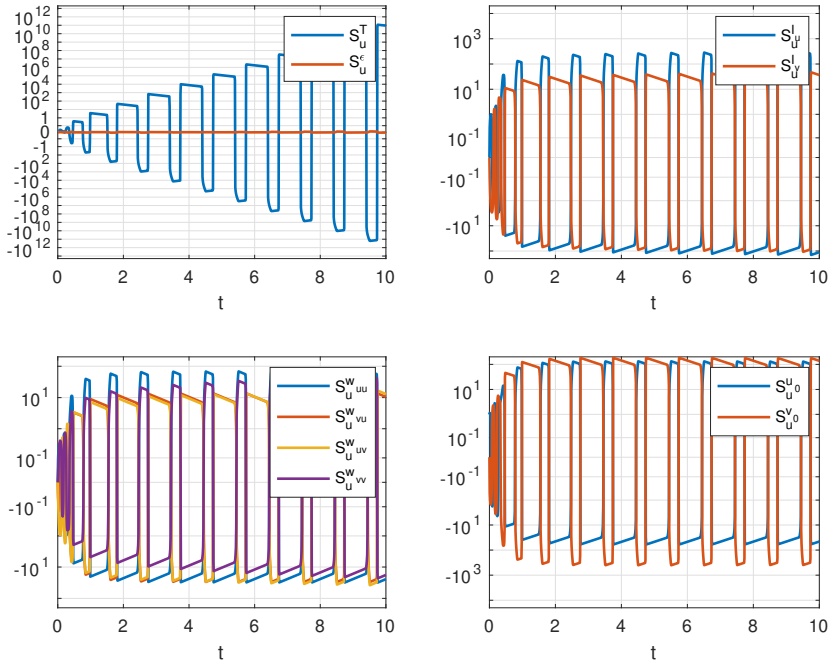

Figure 7: Sensitivity solutions, $S(t)$, in equation (32) with respect to the u population.

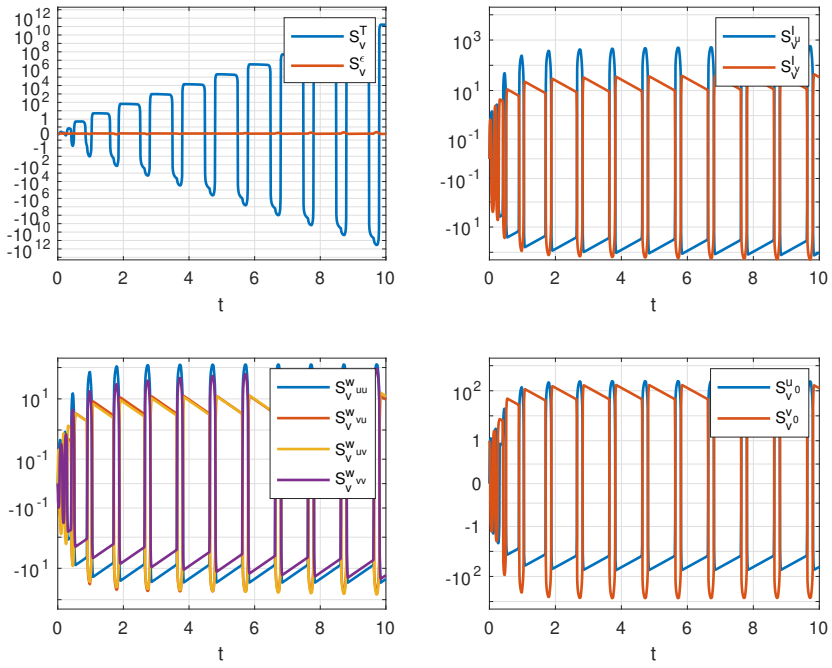

Figure 8: Sensitivity solutions, $S(t)$, in equation (32) with respect to the v population.

each sensitivity function by the associated parameter, p_j, and state variable, $x_i(t,p_0)$. Then, given some state variable values are close to zero, the denominator includes the term +1 to avoid relative sensitivity variables blowing up. As shown in Figures 9 and 10, the behavior of the relative sensitivity functions are similar qualitatively to that of the sensitivity functions, but the use of the relative functions will provide a more fair comparison between variables. For this reason, moving forward we will draw conclusions based on the analysis of the relative sensitivity solutions.

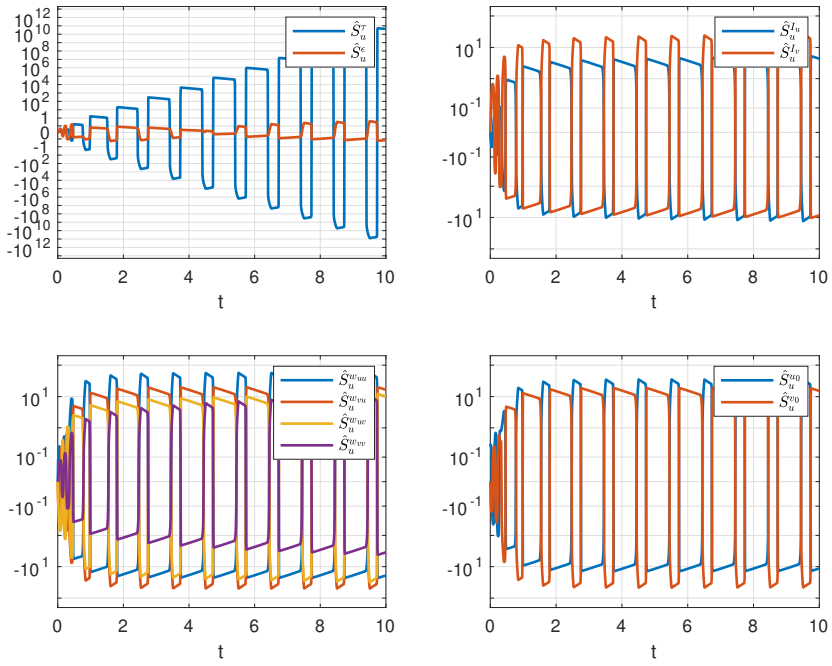

Figure 9: Relative sensitivity solutions, $\hat{S}(t)$, in equation (33) with respect to the u population.

In order to calculate each parameter's influence on the model, we considered the following sensitivity metric for $j = 1,\ldots,10$ (corresponding to the ten parameters in the model as outlined in Table 1) and $i = 1,2$ (corresponding to the two state variables

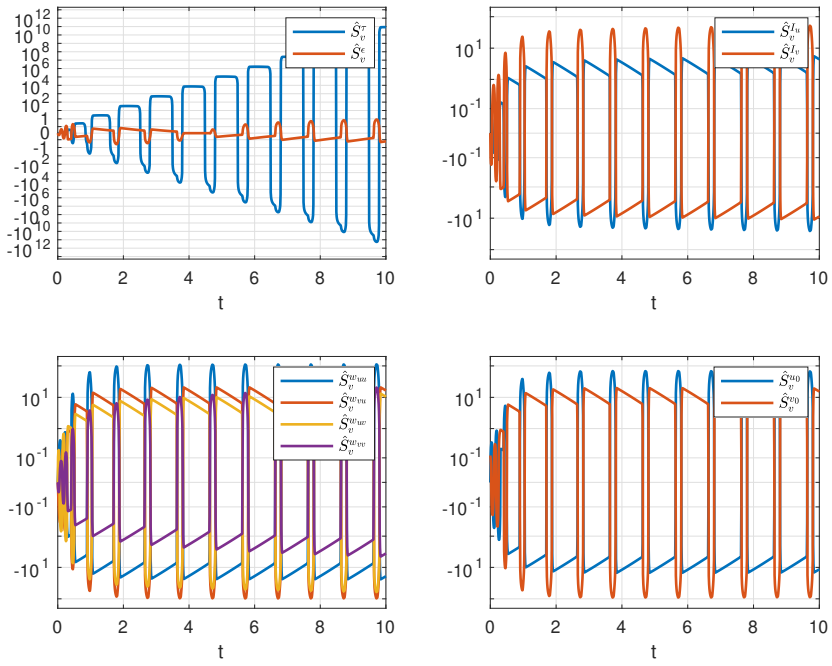

Figure 10: Relative sensitivity solutions, $\hat{S}(t)$, in equation (33) with respect to the v population.

in the model):

$$\|\hat{S}_{x_i}^{p_j}\|_1 = \int_{t_0}^{t_f} |\hat{S}_{x_i}^{p_j}(t)|\, dt\,. \tag{34}$$

This metric integrates across each sensitivity variables from the initial time, $t_0 = 0$, to the final time, $t_f = 10$, which captures the parameter's influence as a scalar value. We then plotted the results so that we could easily determine the most influential parameter (see the bar graph in Figure 11).

Due to the vast differences in parameter influence between each value, we have used a logarithmic scale to portray the results. Based on Figure 11, it is clear to see that the timescale constant, τ, is the most influential parameter to the Nonsmooth Wilson-Cowan model as its parametric influence is greater than 10^{10}, while most other parameters lie in a "mid-tier" level with parametric influences around 10^2. It is also apparent

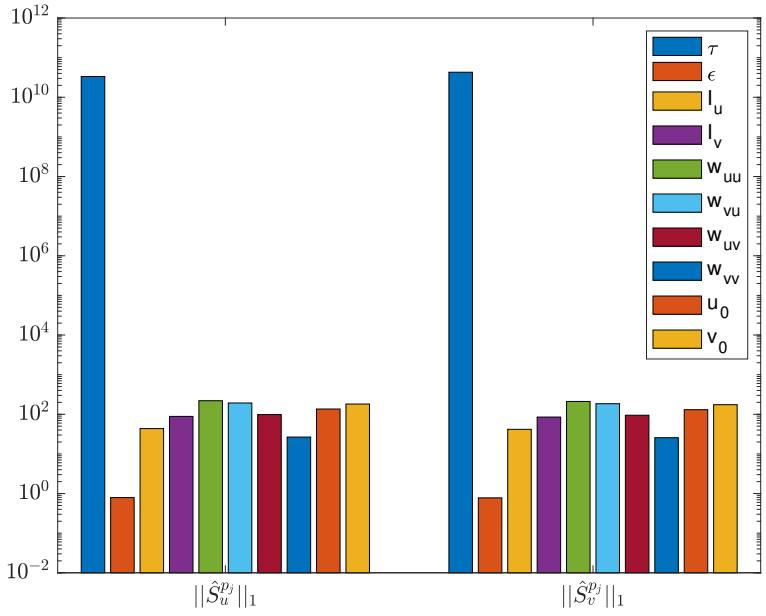

Figure 11: Parametric influence, $\|\hat{S}_{x_i}^{p_j}\|_1$, for different parameters, p_j, and states, x_i, as described in equation (34) to the Nonsmooth Wilson-Cowan model.

that the sharpness factor, ε, is the least influential parameter and lies in the lowest tier with parametric influence less than 1. This implies the proportion of neurons firing per unit time (i.e. the state variables) are not significantly influenced by the gain of the firing rate function. This result is surprising, since we originally hypothesized the model to be notably sensitive to this parameter. Instead, we can conclude that with the chosen parameter values and IC, the rate at which the proportion of neurons firing increases from 0% to 100% is not an influential aspect of the Nonsmooth Wilson-Cowan model, but the timescale constant that determines how much faster the firing rate of inhibitory neurons is relative to excitatory neurons is extremely influential. The next question to investigate is if this result remains true for a range of ICs.

Nonlocal Sensitivity Analysis of Nonsmooth Model

A local sensitivity analysis is specific to one set of ICs and parameters. To capture the parametric influence of the Wilson-Cowan model over a range of initial conditions, a nonlocal sensitivity analysis can be performed. To compute this, we used the influence metric in equation (34) and summed over the influence of each parameter, p_j, across both state variables for some IC (u_0, v_0). This measurement was calculated by

$$H_{j,k} = \sum_{i=1}^{2}\sum_{\ell=1}^{10} ||\hat{S}_{x_i}^{p_\ell}(t)||_1 = \sum_{i=1}^{2}\sum_{\ell=1}^{10} \int_{t_0}^{t_f} |\hat{S}_{x_i}^{p_\ell}(t)|\, dt\,, \tag{35}$$

for the initial condition $(u_0, v_0) = (j,k)$. From there, we created a heatmap (see Figure 12) to represent the influence of all 10 problem parameters across a range of ICs $(u_0, v_0) \in [0,1]^2 = \{(u,v) : 0 \le u \le 1, 0 \le v \le 1\}$.

Based on these, we determined six regions of distinct sensitivity behavior to analyze: Region 1 is the area of the heatmap in the top left (dark purple), Region 2 is the area in the top right (medium purple), Region 3 is the area in the bottom right (light purple), Region 4 is the green area in the bottom left, Region 5 is the orange area in the bottom left, and Region 6 is the yellow area (this is the smallest region). For reference, the ICs used to represent each region in the following figures is marked by a red dot on the heatmap in Figure 12.

The figures below show that varying the initial conditions alters the influence each parameter has on the model. In Region 1 (shown in Figure 13) the behavior of the excitatory neuron population, u, is most sensitive to the initial condition of excitatory

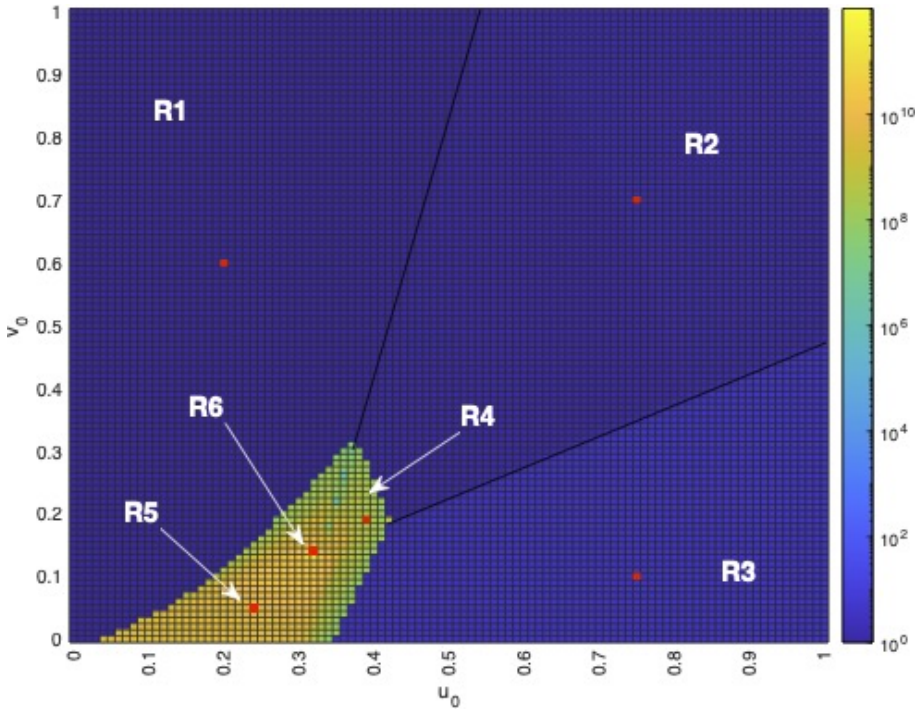

Figure 12: Heatmap of the influence sensitivity metric in equation (35) for different ICs of the Nonsmooth Wilson-Cowan model. Red dots represent ICs used for sensitivity simulations in each region.

neurons, u_0, while the behavior of the inhibitory neuron population, v, is most sensitive to the initial condition of inhibitory neurons, v_0. However, the parametric influence of these parameters takes on values less that 0.3, thus the model is relatively insensitive to all parameters. We believe this is due to the low state variable behavior within this region. Since the ICs seem to be the determining factor of the level of neural activity, it is not surprising that the nonsmooth model is slightly more sensitive to these parameters.

Initial conditions within Regions 2 and 3 follow a similar story to those in Region 1, with a slight increase in state variable behavior, resulting in an increase in parametric influence. The bar graph of Figure 14b shows that u_0 and the the weight of communication between the excitatory population and the inhibitory population, w_{uv}, are the most influential parameters. However, due to the low values of parametric influence overall,

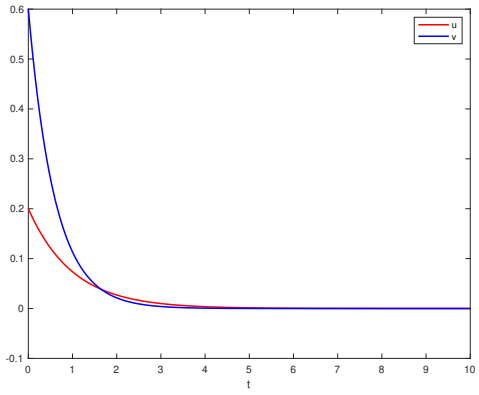

(a) State behavior of u and v.

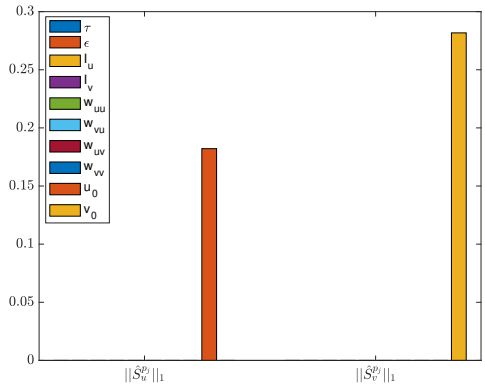

(b) Parametric influences.

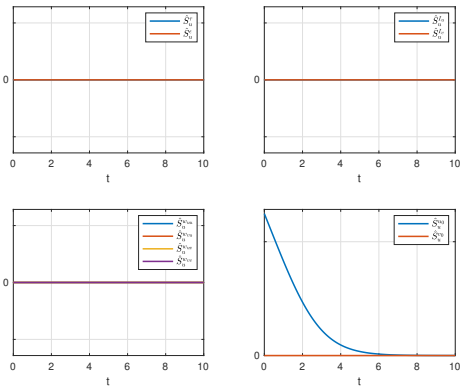

(c) Sensitivity solutions with respect to u.

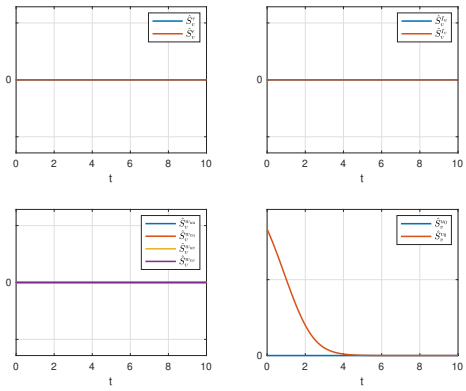

(d) Sensitivity solutions with respect to v.

Figure 13: Sensitivity analysis of ICs in Region 1 of the Nonsmooth Wilson-Cowan model.

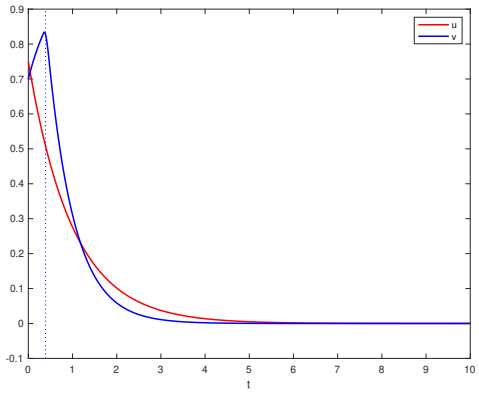

(a) State behavior of u and v.

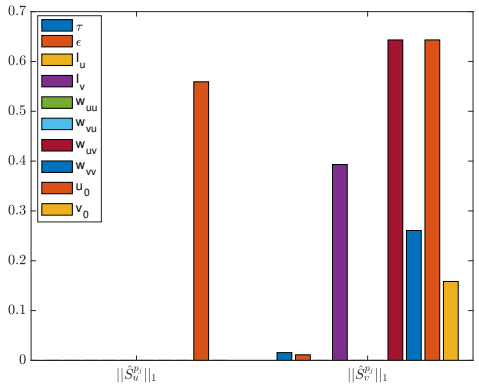

(b) Parametric influences.

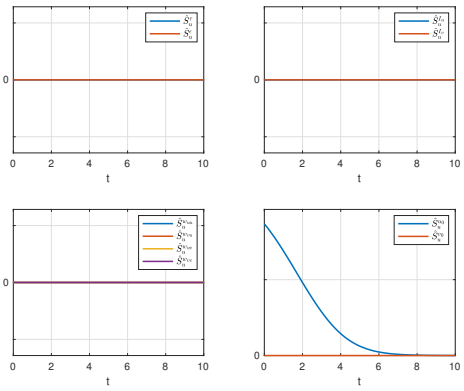

(c) Sensitivity solutions with respect to u.

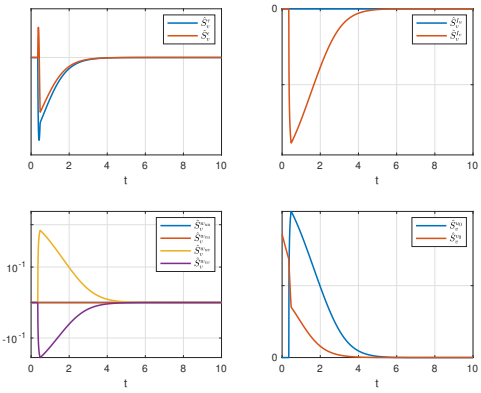

(d) Sensitivity solutions with respect to v.

Figure 14: Sensitivity analysis of ICs in Region 2 of the Nonsmooth Wilson-Cowan model.

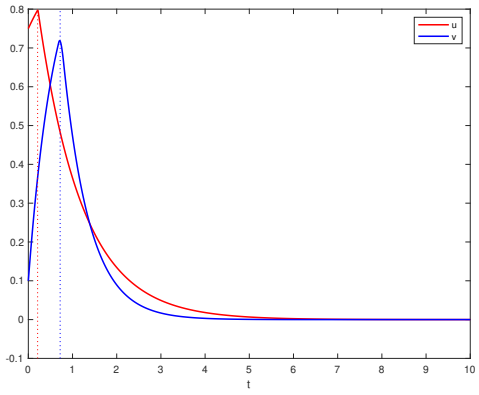

(a) State behavior of u and v.

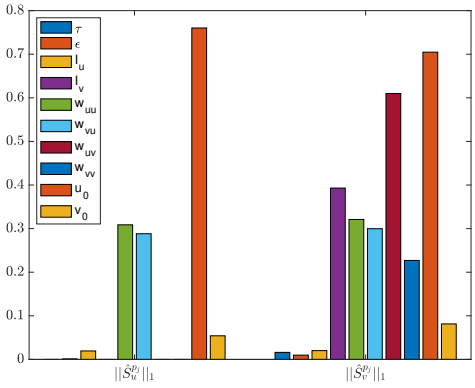

(b) Parametric influences.

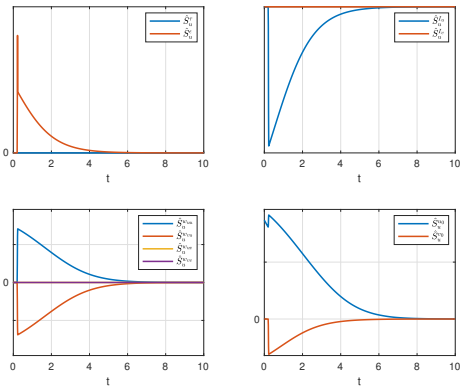

(c) Sensitivity solutions with respect to u.

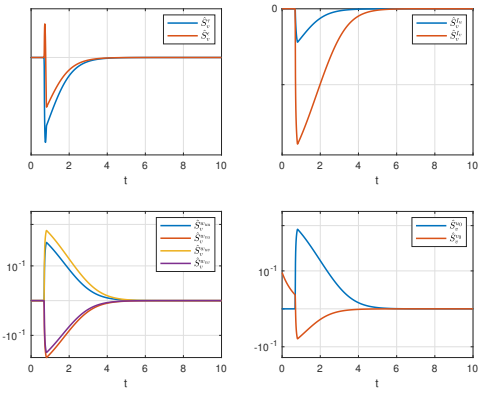

(d) Sensitivity solutions with respect to v.

Figure 15: Sensitivity analysis of ICs in Region 3 of the Nonsmooth Wilson-Cowan model.

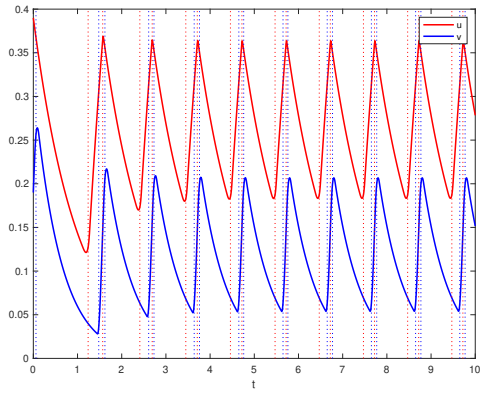

(a) State behavior of u and v.

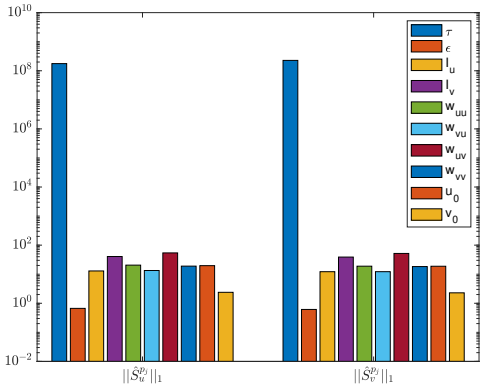

(b) Parametric influences.

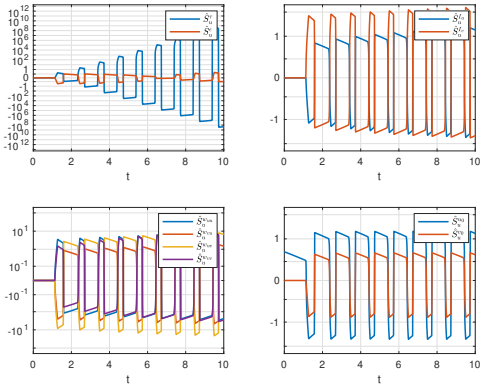

(c) Sensitivity solutions with respect to u.

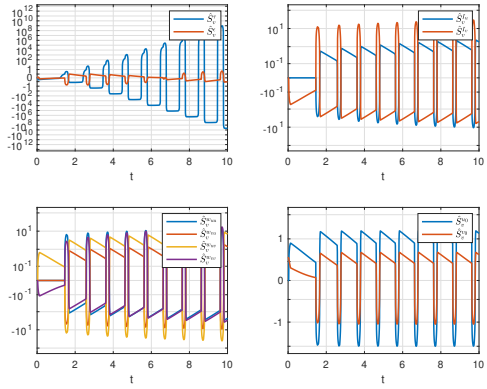

(d) Sensitivity solutions with respect to v.

Figure 16: Sensitivity analysis of ICs in Region 4 of the Nonsmooth Wilson-Cowan model.

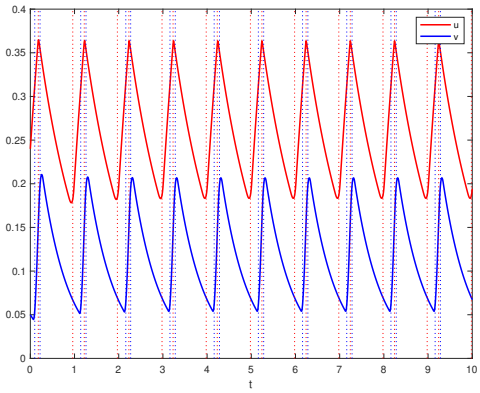

(a) State behavior of u and v.

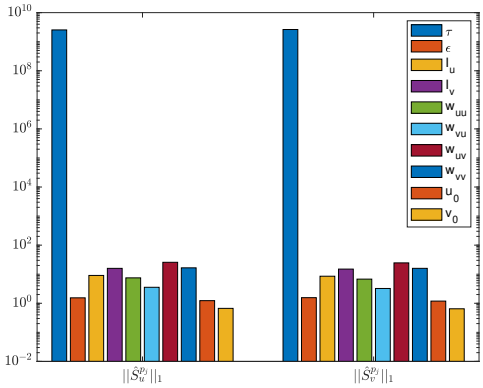

(b) Parametric influences.

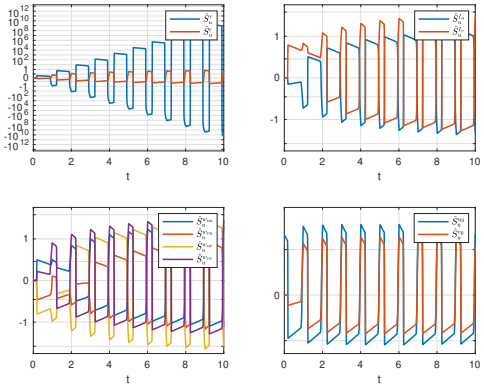

(c) Sensitivity solutions with respect to u.

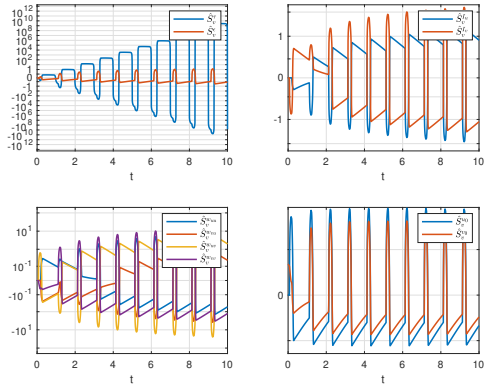

(d) Sensitivity solutions with respect to v.

Figure 17: Sensitivity analysis of ICs in Region 5 of the Nonsmooth Wilson-Cowan model.

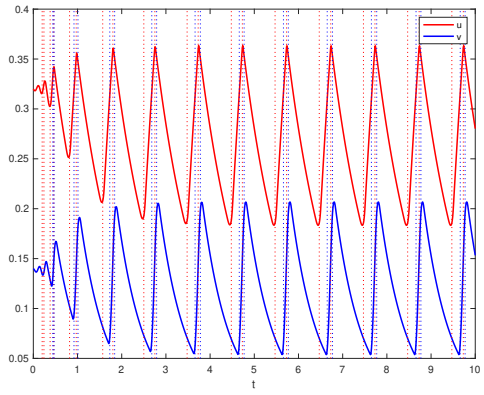

(a) State behavior of u and v.

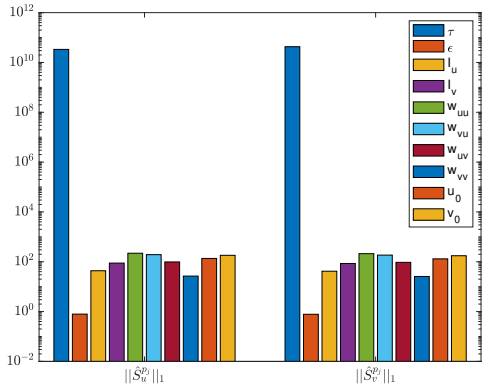

(b) Parametric influences.

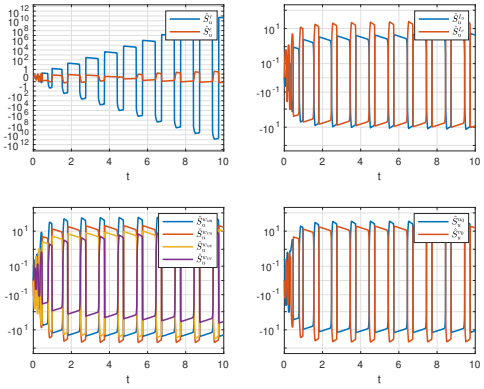

(c) Sensitivity solutions with respect to u.

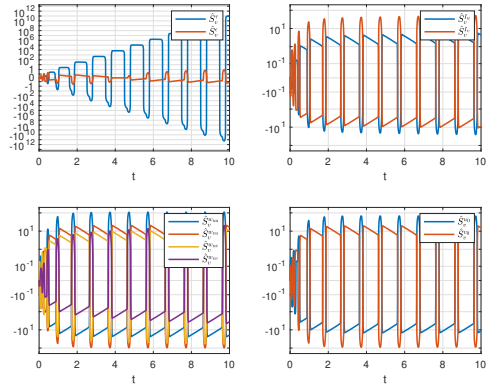

(d) Sensitivity solutions with respect to v.

Figure 18: Sensitivity analysis of ICs in Region 6 of the Nonsmooth Wilson-Cowan model.

the model continues to be relatively insensitive to all parameters, which supports the idea that in regions of low state variable activity, the model is fairly insensitive to all parameters.

Regions 4, 5, and 6 are made up of initial conditions that exhibit high state variable behavior. As shown in Figure 16a, a spiking behavior is present. This seems to indicate that groups of neurons are firing more frequently than in other regions, which implies there is a balance between the amount of excitation and inhibition of neurons within the network. This balance results in a repeated pattern of an increase in the proportion of firing neurons in each population followed by a decrease in the proportion of firing neurons, building the repeated spikes shown in the figure. As shown by the bar graphs of Figures 16b, 17b, and 18b, the timescale constant, τ, is the most influential parameter of these regions. The distinguishing factor of these regions is the magnitude of model sensitivity to this parameter, since Regions 4 and 5 are less sensitive to τ than Region 6. In regards to other parameters, most of them lie in a similar "mid-tier" level of influence as described in our discussion of the local sensitivity analysis, with the sharpness factor of the firing rate function, ε, remaining the least influential parameter.

Comparison to Sensitivity Analysis of Smooth Model

A sensitivity analysis of the Smooth Wilson-Cowan model can be performed using classic ODE theory since all equations are smooth. Here, let $f^*(p_0, x(t, p_0))$ be the right hand side function of the Wilson-Cowan ODE system using the smooth firing rate function of equation (23) and $S^*(t)$ be the 2×10 solutions matrix of the smooth sensitivity

equations, which is denoted

$$S^*(t) = \begin{bmatrix} \frac{\partial u}{\partial p}(t, p_0) \\ \frac{\partial v}{\partial p}(t, p_0) \end{bmatrix} = \begin{bmatrix} S_u^*(t, p_0) \\ S_v^*(t, p_0) \end{bmatrix},$$

where an asterisk is used to distinguish between the nonsmooth sensitivity variables and the smooth variables. Then, as explained in Chapter II, the sensitivity equations of the smooth model are found using equation (3) and thus are calculated by,

$$\begin{aligned} \dot{S}^*(t) &= J_p f(p_0, x(t, p_0)) + J_x f(p_0, x(t, p_0))\, S^*(t) \\ &= \begin{bmatrix} \frac{\partial (F_u^*)}{\partial p} \\ \frac{\partial (F_v^*)}{\partial p} \end{bmatrix} + \begin{bmatrix} \frac{\partial (F_u^*)}{\partial x} \\ \frac{\partial (F_v^*)}{\partial x} \end{bmatrix} \begin{bmatrix} S_u^*(t) \\ S_v^*(t) \end{bmatrix} \\ &= \begin{bmatrix} \frac{\partial F_u^*}{\partial p_1} & \frac{\partial F_u^*}{\partial p_2} & \cdots & \frac{\partial F_u^*}{\partial p_{10}} \\ \frac{\partial F_v^*}{\partial p_1} & \frac{\partial F_v^*}{\partial p_2} & \cdots & \frac{\partial F_v^*}{\partial p_{10}} \end{bmatrix} + \begin{bmatrix} \frac{\partial F_u^*}{\partial u} & \frac{\partial F_u^*}{\partial v} \\ \frac{\partial F_v^*}{\partial u} & \frac{\partial F_v^*}{\partial v} \end{bmatrix} \begin{bmatrix} S_u^*(t) \\ S_v^*(t) \end{bmatrix} \\ &= \begin{bmatrix} F_u^{*\prime} \\ F_v^{*\prime} \end{bmatrix} + \begin{bmatrix} -1 + \frac{\varepsilon w_{uu} e^{-\varepsilon(x_u)}}{(1+e^{-\varepsilon(x_u)})^2} & -\frac{\varepsilon w_{vu} e^{-\varepsilon(x_u)}}{(1+e^{-\varepsilon(x_u)})^2} \\ \frac{\varepsilon w_{uv} e^{-\varepsilon(x_v)}}{(1+e^{-\varepsilon(x_v)})^2} & -\frac{1}{\tau} - \frac{\varepsilon w_{vu} e^{-\varepsilon(x_v)}}{\tau(1+e^{-\varepsilon(x_v)})^2} \end{bmatrix} \begin{bmatrix} S_u^*(t) \\ S_v^*(t) \end{bmatrix}, \end{aligned} \tag{36}$$

using the variables in Table 3 for simplicity and the fact that

$$\text{expit}'(x) = \frac{e^x}{(1+e^x)^2} = \text{expit}(x)(1 - \text{expit}(x)).$$

Smooth Sensitivity Equation Auxiliary Variables	
Symbol	Expression
x_u	$I_u + w_{uu}u - w_{vu}v$
x_v	$I_v + w_{uv}u - w_{vv}v$
F_u^*	$-u + \frac{1}{1+e^{-\varepsilon(x_u)}}$
F_v^*	$-v + \frac{1}{1+e^{-\varepsilon(x_v)}}$
$F_u^{*'}$	$\text{expit}'(x_u)\begin{bmatrix} 0 & -(x_u) & \varepsilon & 0 & \varepsilon(u) & -\varepsilon(v) & 0 & 0 & 0 & 0 \end{bmatrix}$
$F_v^{*'}$	$\frac{\text{expit}'(x_v)}{\tau}\begin{bmatrix} -\frac{(1+e^{-\varepsilon(x_v)})}{\tau(e^{-\varepsilon(x_v)})} & -(x_v) & 0 & \varepsilon & 0 & 0 & \varepsilon(u) & -\varepsilon(v) & 0 & 0 \end{bmatrix}$

Table 3: Variables in equation (36) that simplify the derivation of the Smooth Wilson-Cowan sensitivity equations.

Therefore the sensitivity equations of the smooth Wilson-Cowan model are,

$$\begin{aligned}
\dot{S}_u^* &= F_u^{*'} - S_u^* + \left(\frac{\varepsilon w_{uu} e^{-\varepsilon(x_u)}}{(1+e^{-\varepsilon(x_u)})^2}\right) S_u^* - \left(\frac{\varepsilon w_{vu} e^{-\varepsilon(x_u)}}{(1+e^{-\varepsilon(x_u)})^2}\right) S_u^*, \\
\dot{S}_v^* &= F_v^{*'} + \left(\frac{\varepsilon w_{uv} e^{-\varepsilon(x_v)}}{(1+e^{-\varepsilon(x_v)})^2}\right) S_v^* - \left(\frac{1}{\tau}\right) S_v^* + - \left(\frac{\varepsilon w_{vu} e^{-\varepsilon(x_v)}}{\tau(1+e^{-\varepsilon(x_v)})^2}\right) S_v^*, \\
S_u^*(t_0) &= \begin{bmatrix} \mathbf{0}_{1\times 8} & 1 & 0 \end{bmatrix}, \\
S_v^*(t_0) &= \begin{bmatrix} \mathbf{0}_{1\times 8} & 0 & 1 \end{bmatrix}.
\end{aligned} \tag{37}$$

For a local sensitivity analysis, we used the parameter values found in Table 1 to simulate the smooth relative sensitivity equations and calculated the parametric influence using equation (34), which is shown in Figure 19. In contrast to the nonsmooth model, the timescale constant, τ, is the least influential parameter to the smooth model. Since τ reflects how much quicker the inhibitory neurons are firing in comparison to the excitatory neurons, these results imply that the Smooth Wilson-Cowan model is relatively insensitive to changes in the timescale on which v is functioning on. Instead, the smooth model is sensitive to parameters such as external signals inputting to the

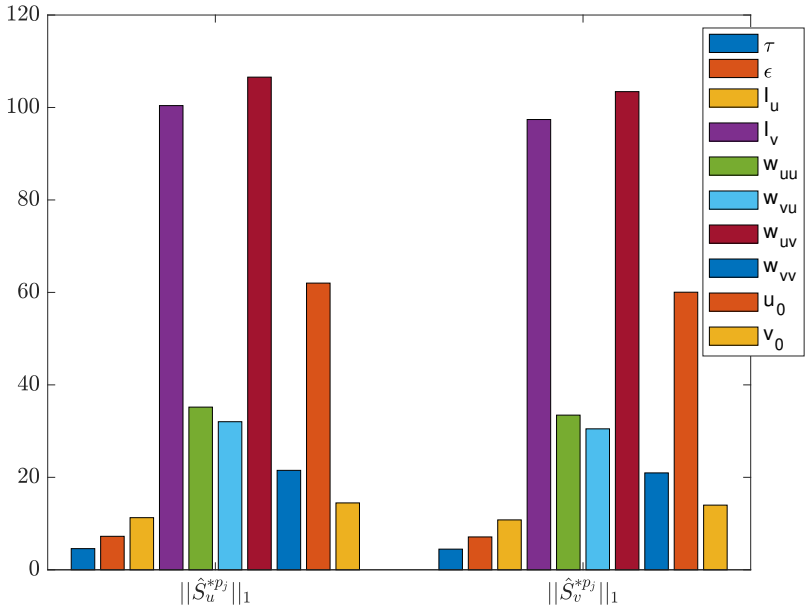

Figure 19: Parametric influence, $||\hat{S}_{x_i}^{*p_j}||_1$, for different parameters, p_j, and states, x_1, as described in equation (34) to the Smooth Wilson-Cowan Model.

v population, I_v, and the weight of the synapse between the excitatory and inhibitory populations, w_{uv}. Therefore, local sensitivity results about the smooth model do not match the results of the nonsmooth model.

Next, we created a heatmap displaying the sum of each parametric influence for each p_j and state variable x_i for a range of ICs, which is calculated by equation (35) (see Figure 20). The heatmap showed that most initial conditions of the smooth model resulted in low levels of parametric influence in comparison to the nonsmooth model. Additionally, there is primarily one region of distinct sensitivity behavior, which indicates that the smooth model is equally sensitive to the model parameters across most initial conditions. Nonetheless, we analyzed the smooth model's sensitivity information for ICs in the six regions found in the nonlocal sensitivity analysis of the nonsmooth model in order to gain a complete comparison, which is shown in the figures below.

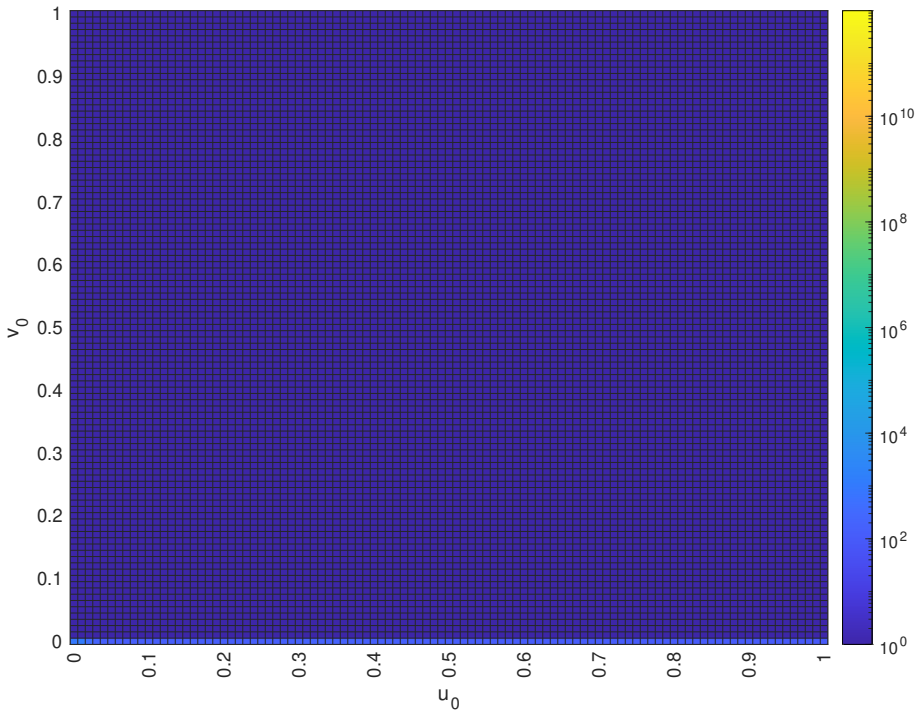

Figure 20: Heatmap of the influence sensitivity metric in equation (35) for different ICs of the Smooth Wilson-Cowan model.

What stood out the most when analyzing the sensitivity information of the smooth model was the fact that in regions of spiking behavior (i.e. Regions 4, 5, and 6) the state variable behavior within each region was qualitatively similar to that of the state variable behavior of the nonsmooth model, but that the sensitivity solutions differ. For example, in Region 6, the state variable activity of the smooth model spike in a similar way to the nonsmooth model, just at a slightly later time (see Figure 27), while the sensitivities within this region appear slightly different in the smooth model than in the nonsmooth, as discussed previously.

To further investigate the differences between both models, we created heatmaps comparing the state variables between the smooth and nonsmooth models as well as heatmaps comparing the sensitivity behavior between the smooth and nonsmooth mod-

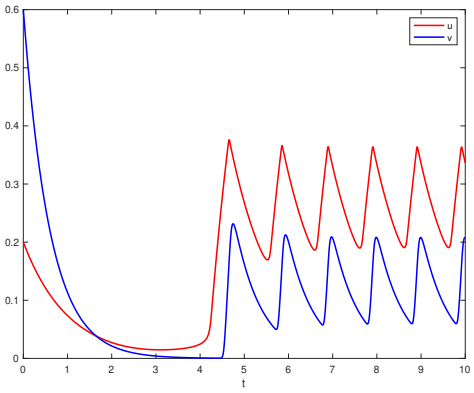

(a) State behavior of u and v.

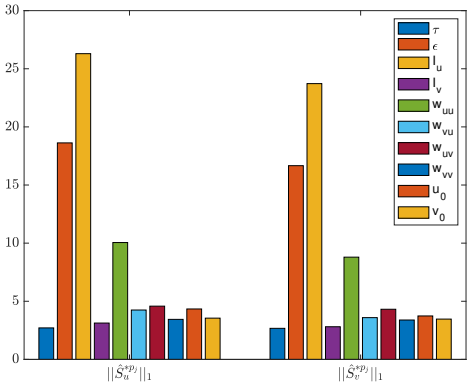

(b) Parametric influences.

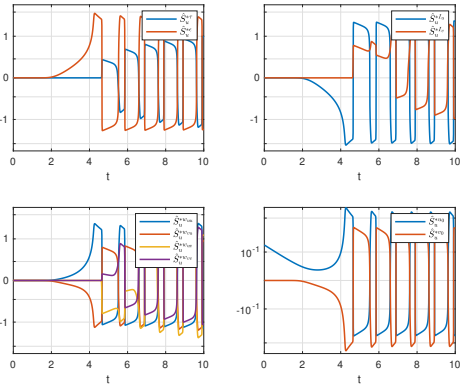

(c) Sensitivity solutions with respect to u.

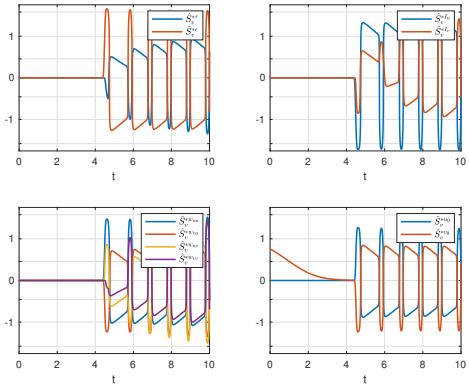

(d) Sensitivity solutions with respect to v.

Figure 21: Sensitivity analysis of ICs in Region 1 of the Smooth Wilson-Cowan model.

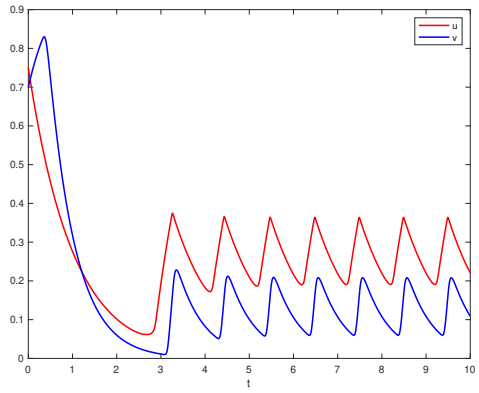

(a) State behavior of u and v.

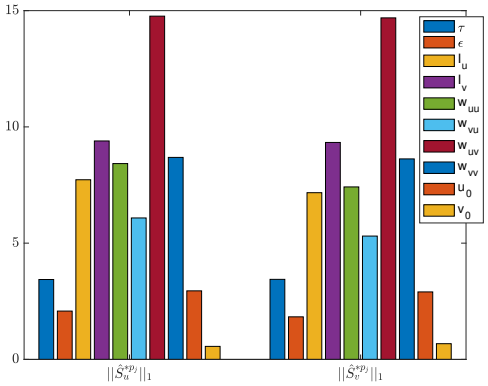

(b) Parametric influences.

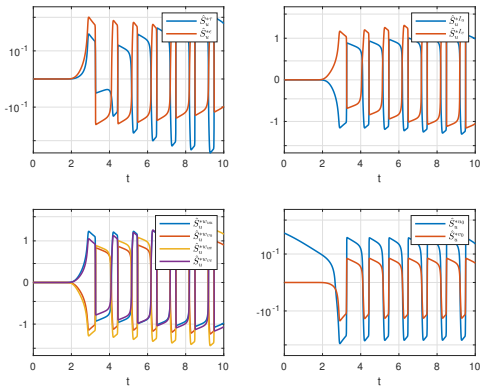

(c) Sensitivity solutions with respect to u.

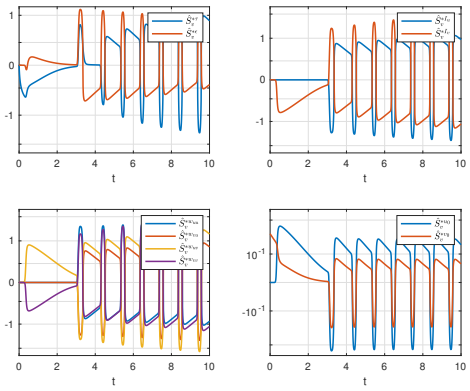

(d) Sensitivity solutions with respect to v.

Figure 22: Sensitivity analysis of ICs in Region 2 of the Smooth Wilson-Cowan model.

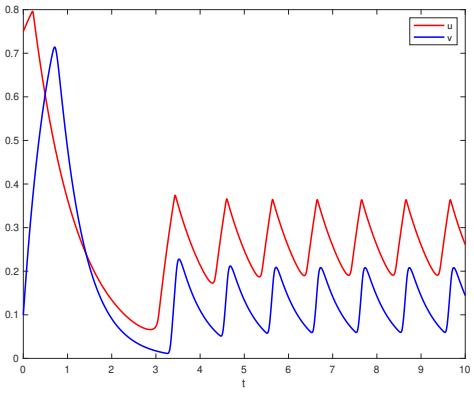

(a) State behavior of u and v.

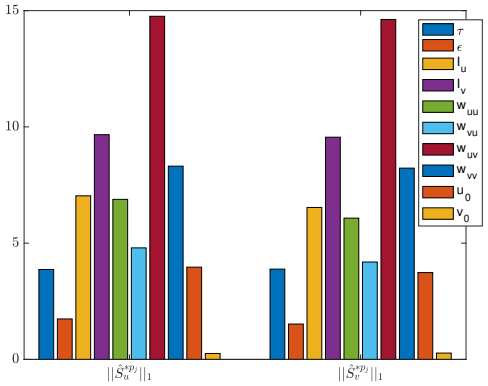

(b) Parametric influences.

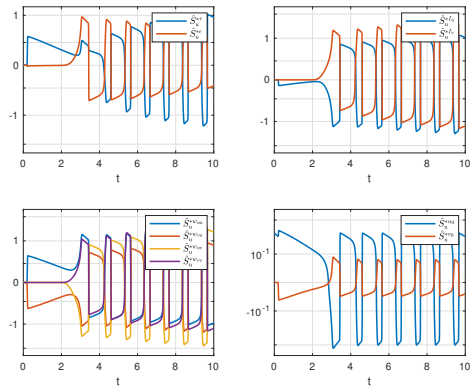

(c) Sensitivity solutions with respect to u.

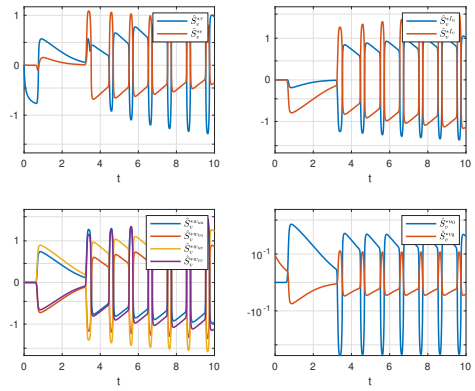

(d) Sensitivity solutions with respect to v.

Figure 23: Sensitivity analysis of ICs in Region 3 of the Smooth Wilson-Cowan model.

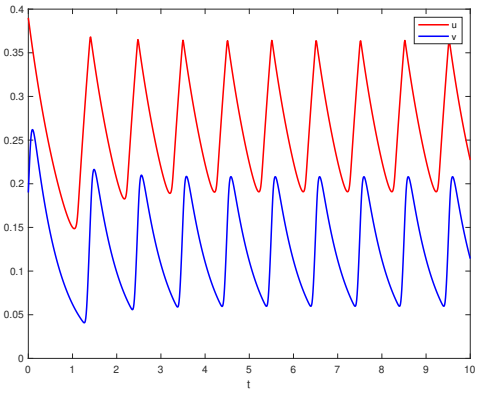

(a) State behavior of u and v.

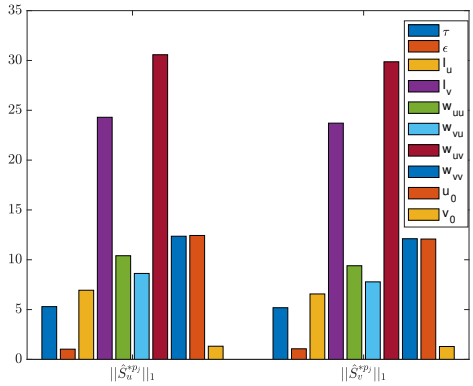

(b) Parametric influences.

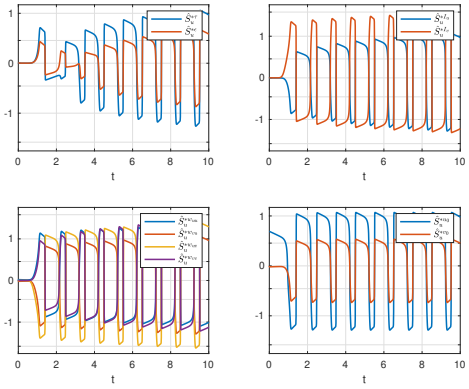

(c) Sensitivity solutions with respect to u.

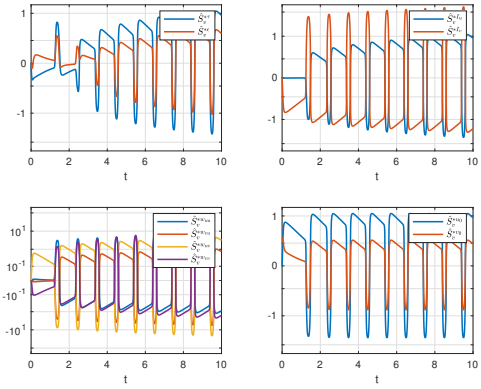

(d) Sensitivity solutions with respect to v.

Figure 24: Sensitivity analysis of ICs in Region 4 of the Smooth Wilson-Cowan model.

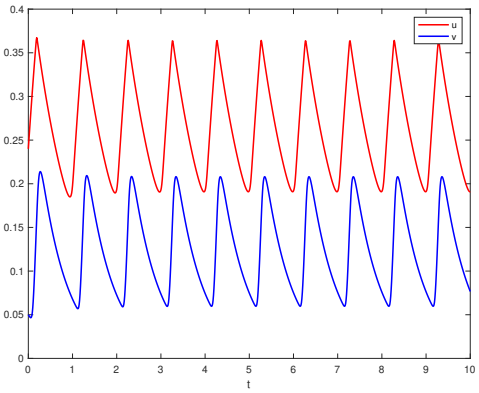

(a) State behavior of u and v.

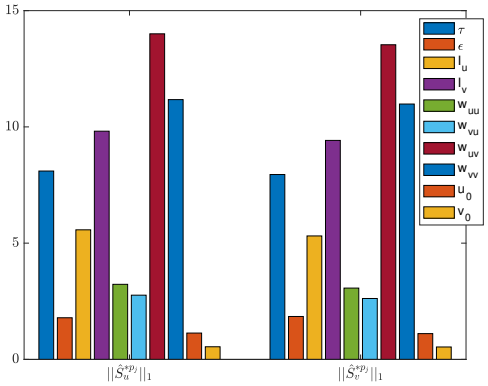

(b) Parametric influences.

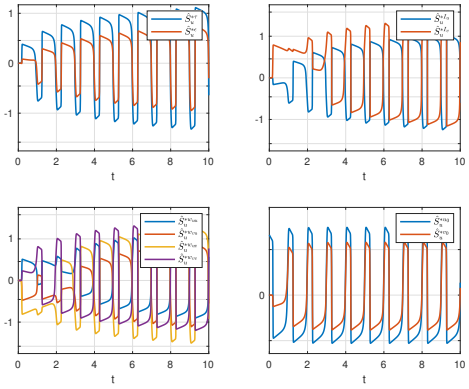

(c) Sensitivity solutions with respect to u.

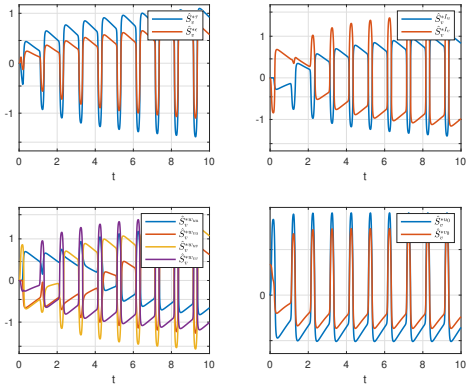

(d) Sensitivity solutions with respect to v.

Figure 25: Sensitivity analysis of ICs in Region 5 of the Smooth Wilson-Cowan model.

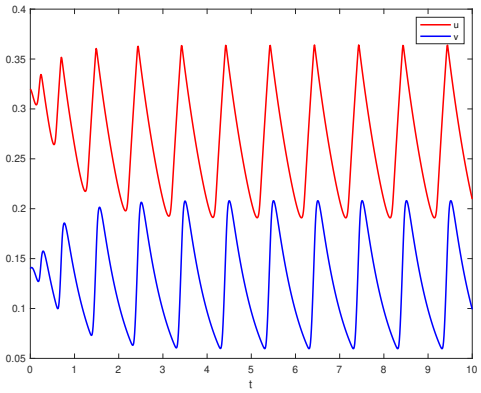

(a) State behavior of u and v.

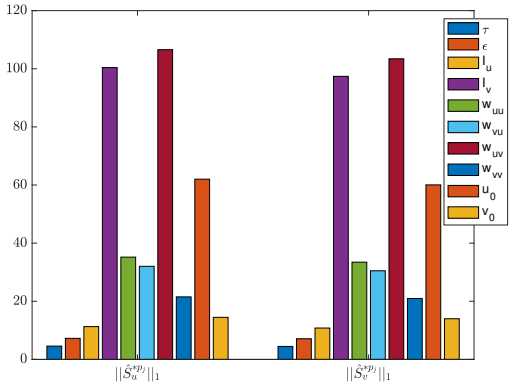

(b) Parametric influences.

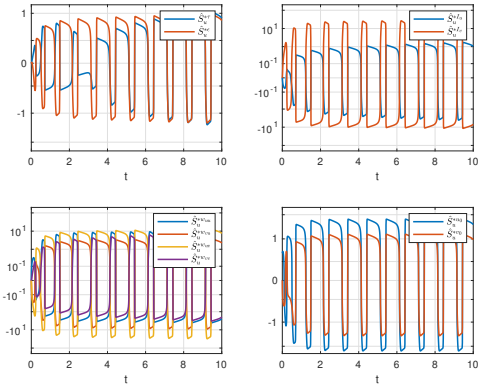

(c) Sensitivity solutions with respect to u.

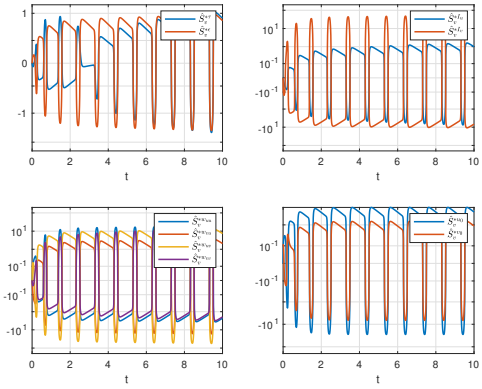

(d) Sensitivity solutions with respect to v.

Figure 26: Sensitivity analysis of ICs in Region 6 of the Smooth Wilson-Cowan model.

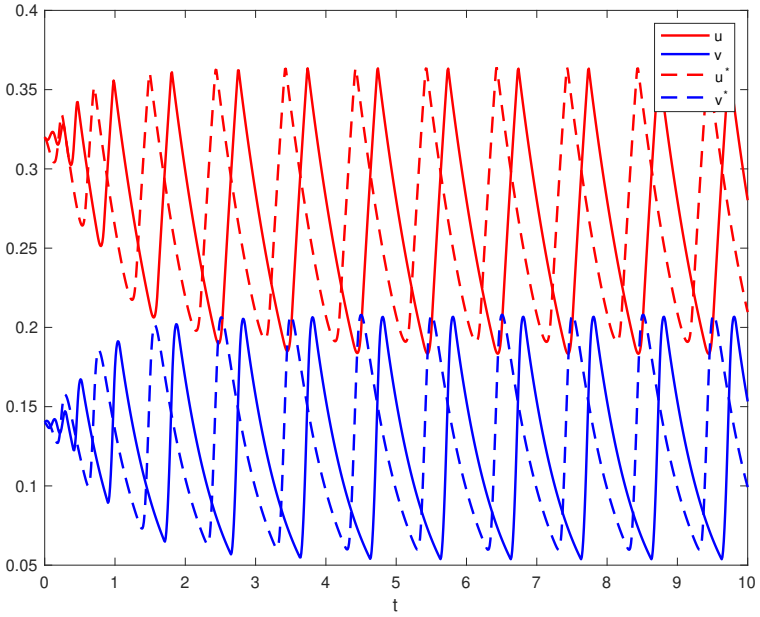

Figure 27: State variable behavior of ICs in Region 6 in both the Smooth and Nonsmooth Wilson-Cowan models.

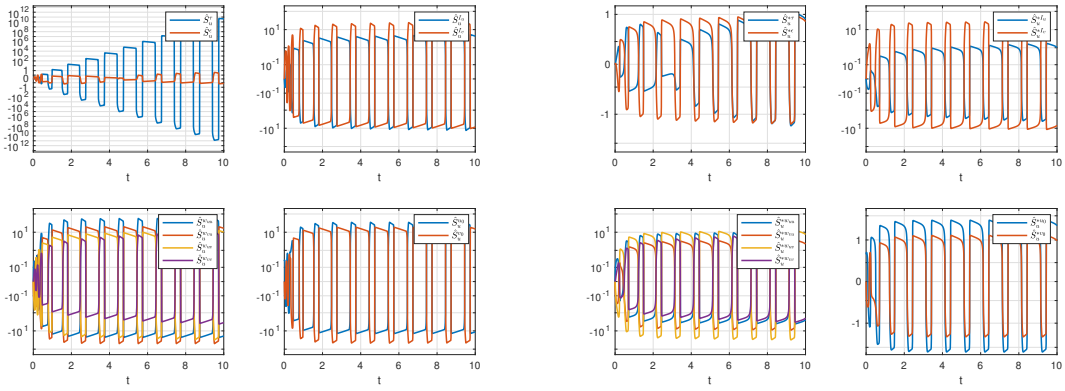

(a) Sensitivities of the Nonsmooth model.

(b) Sensitivities of the Smooth model.

Figure 28: Sensitivity behavior with respect to the u population of ICs within Region 6 of both the Smooth and Nonsmooth Wilson-Cowan models.

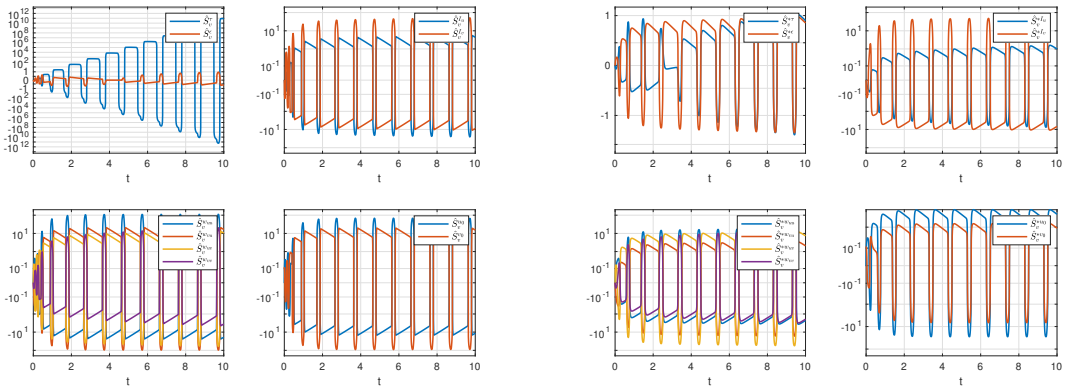

(a) Sensitivities of the Nonsmooth model.

(b) Sensitivities of the Smooth model.

Figure 29: Sensitivity behavior with respect to the v population of ICs within Region 6 of both the Smooth and Nonsmooth Wilson-Cowan models.

els. In the following calculations, define the Wilson-Cowan smooth model state variable solutions as elements of the matrix $X^*(i,j)$ and the nonsmooth model state variable solution as elements of the matrix $X(i,j)$ where

$$X^*(i,j) = \begin{bmatrix} u^*(t_0) & v^*(t_0) \\ u^*(t_1) & v^*(t_1) \\ \vdots & \vdots \\ u^*(t_f) & v^*(t_f) \end{bmatrix} \text{ and } X(i,j) = \begin{bmatrix} u(t_0) & v(t_0) \\ u(t_1) & v(t_1) \\ \vdots & \vdots \\ u(t_f) & v(t_f) \end{bmatrix}$$

from the initial time, t_0, to the final time, t_f with the index (i,j) that is determined by the initial condition, (u_0, v_0). The difference between state variable behavior of the Wilson-Cowan model with a smooth and nonsmooth firing rate is then calculated by

$$C_{i,j}^{states} = \frac{||X(i,j) - X^*(i,j)||_1}{||X(i,j)||_1}. \tag{38}$$

To compare the sensitivity behavior, define the Wilson-Cowan smooth model sensitivity solutions as elements of the matrix $S^*(i,j)$ and the nonsmooth model sensitivity solutions as elements of the matrix $S(i,j)$ where

$$S^*(i,j) = \begin{bmatrix} S_u^{*p_1}(t_0) & \dots & S_u^{*p_{10}}(t_0) & S_v^{*p_1}(t_0) & \dots & S_v^{*p_{10}}(t_0) \\ S_u^{*p_1}(t_1) & \dots & S_u^{*p_{10}}(t_1) & S_v^{*p_1}(t_1) & \dots & S_v^{*p_{10}}(t_1) \\ \vdots & \ddots & \vdots & \vdots & \ddots & \vdots \\ S_u^{*p_1}(t_f) & \dots & S_u^{*p_{10}}(t_f) & S_v^{*p_1}(t_f) & \dots & S_v^{*p_{10}}(t_f) \end{bmatrix}$$

and

$$S(i,j) = \begin{bmatrix} S_u^{p_1}(t_0) & \dots & S_u^{p_{10}}(t_0) & S_v^{p_1}(t_0) & \dots & S_v^{p_{10}}(t_0) \\ S_u^{p_1}(t_1) & \dots & S_u^{p_{10}}(t_1) & S_v^{p_1}(t_1) & \dots & S_v^{p_{10}}(t_1) \\ \vdots & \ddots & \vdots & \vdots & \ddots & \vdots \\ S_u^{p_1}(t_f) & \dots & S_u^{p_{10}}(t_f) & S_v^{p_1}(t_f) & \dots & S_v^{p_{10}}(t_f) \end{bmatrix},$$

once again from the initial time, t_0, to the final time, t_f, with the index $(i,j) = (u_0, v_0)$. Therefore, the difference between sensitivity behavior of the Wilson-Cowan model with a smooth and nonsmooth firing rate, $C_{i,j}^{sens}$, is calculated by

$$C_{i,j}^{sens} = \frac{||S(i,j) - S^*(i,j)||_1}{||S(i,j)||_1}. \tag{39}$$

We then computed $C_{i,j}^{states}$ and $C_{i,j}^{sens}$ across initial conditions (u_0, v_0) in $[0,1]^2$ to produce the heatmaps in Figure 30. As shown in these images, the difference in state variable behavior is relatively low compared to the difference in sensitivity behavior.

The similarity in state variable behavior supports the idea that the Nonsmooth Wilson-Cowan model resembles the smooth model studied in the literature, but the slight difference in the timing of the spikes indicates the need to study both models.

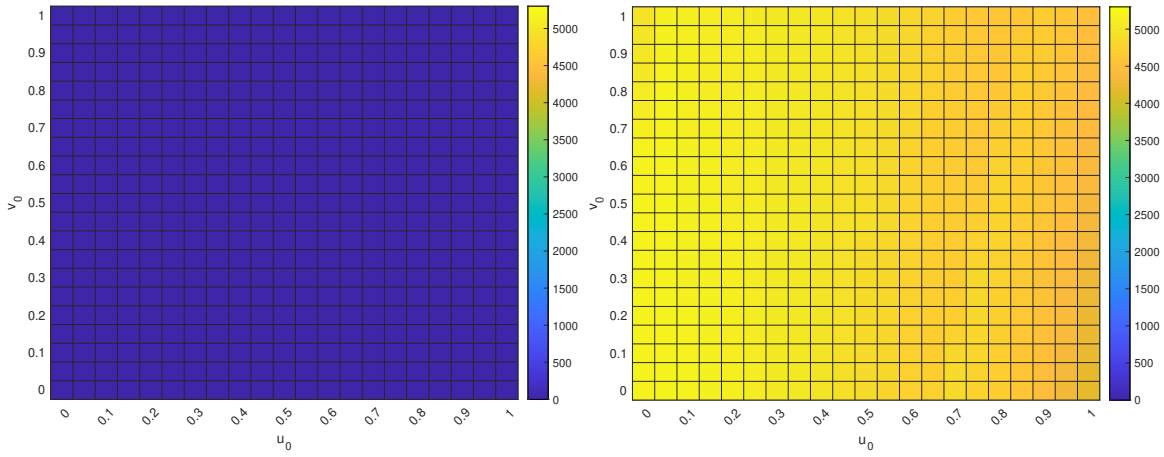

(a) Heatmap of $C_{i,j}^{states}$.

(b) Heatmap of $C_{i,j}^{sens}$.

Figure 30: Heatmaps comparing state variable and sensitivity behavior between the smooth model and the nonsmooth model with PWL firing rate function in (25).

In addition to this, the difference in sensitivity solutions between the two models gives rise to many questions about which model better suits the dynamics of the neuron populations the Wilson-Cowan neural mass model is aiming to capture. Though we have made no concrete conclusions about which model achieves this, the fact that the smooth model has been questioned in terms of how biologically accurate it is to the "on/off" behavior of firing neurons indicates that any conclusions made based on the sensitivity of the smooth model may not reflect the true biological phenomena of this neural network.

Although the state variable behavior appears similar, differences remain between the smooth and nonsmooth models. As shown in Figure 31, initial conditions within Regions 1 result in the state variables of the nonsmooth model to approach the point $(u,v) = (0,0)$ while the state variables of the smooth model exhibit a spiking behavior after a period of time. Furthermore, this is true for initial conditions within regions 2 and 3, implying all initial conditions exhibit a spiking behavior of the states. Consider-

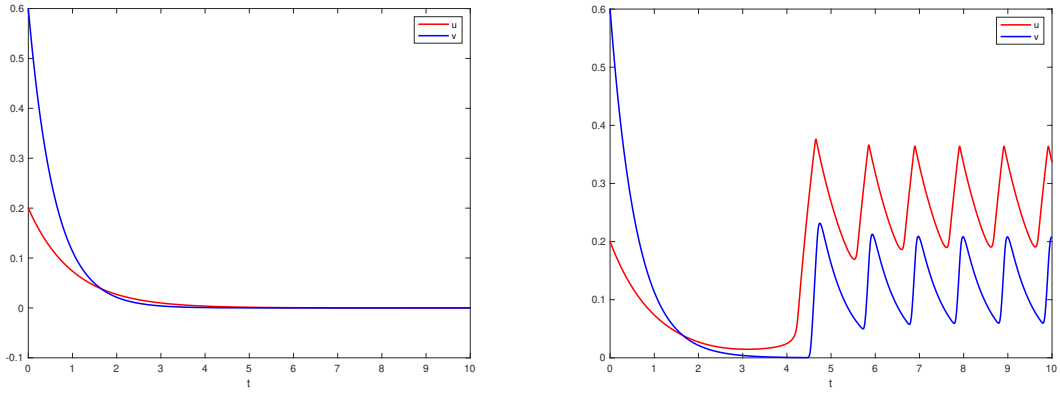

(a) State variable behavior of u and v populations of the Nonsmooth model.

(b) State variable behavior of u and v populations of the Smooth model.

Figure 31: State variable behavior of ICs in Region 1 in both the Smooth and Nonsmooth Wilson-Cowan models.

ing what is going on here motivates questions about the long-term behavior of the state variables, which can be answered by performing a stability analysis of both the smooth and nonsmooth models.

CHAPTER V

STABILITY ANALYSIS

Equilibria and Limit Cycles of Nonsmooth Model

The ODEs of the Wilson-Cowan Model in equation (22) describe the change in state variable behavior, u and v. Therefore, when the right-hand side of these equations are equal to zero there is no change in state variable behavior. Thus any equilibria, (u,v), is calculated by solving the nonlinear equation system

$$\begin{aligned} \dot{u} = 0 &= -u + F(I_u + w_{uu}u - w_{vu}v), \\ \dot{v} = 0 &= \frac{1}{\tau}[-v + F(I_v + w_{uv}u - w_{vv}v)]. \end{aligned} \tag{40}$$

In order to get a sense of the equilibria of the nonsmooth Wilson-Cowan model, we first analyzed phase portraits of the model, which provided information on the relationship between the excitatory and inhibitory neuron populations. As shown in red in Figure 32, there appears to be two equilibria and one limit cycle (similar to the limit cycle found in [5]), based on the flow of trajectories. We will denote the equilibrium located to the left of the portrait (u_1, v_1) and the equilibrium inside the limit cycle (u_2, v_2). We now want to verify the presence of these points analytically or numerically.

The blue and green dashed lines in Figure 32 represent the switching manifolds, which are when the firing rate function in equation (25) crosses into a new input argu-

ment, implying the function is now using a different piece of the PWL nonsmooth firing rate function. These switching manifolds are calculated by,

$$\begin{aligned}\left\{(u,v): I_u + w_{uu}u - w_{vu}v = -\frac{2}{\varepsilon}, \frac{2}{\varepsilon}\right\},\\ \left\{(u,v): I_v + w_{uv}u - w_{vv}v = -\frac{2}{\varepsilon}, \frac{2}{\varepsilon}\right\},\end{aligned} \tag{41}$$

since these are the bounds of the PWL firing rate function.

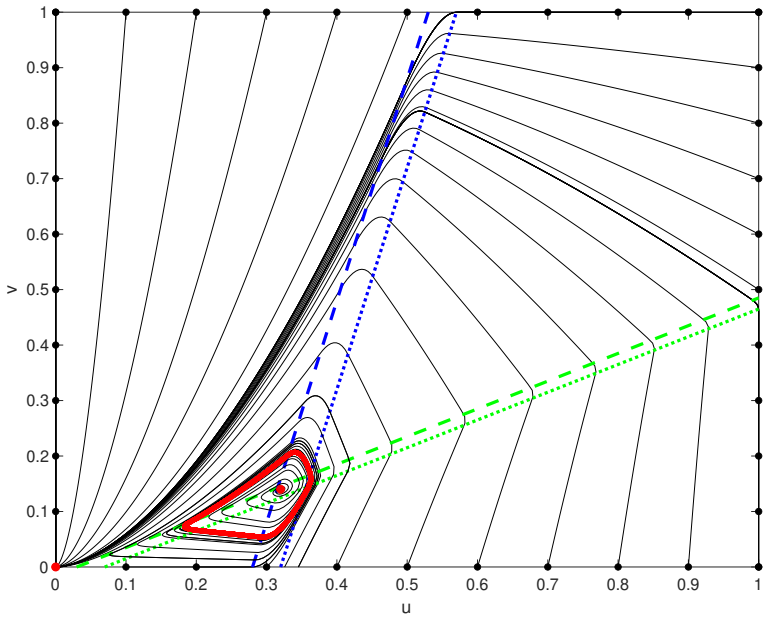

Figure 32: Phase portrait of the Nonsmooth Wilson-Cowan model. Blue and green dashed lines correspond to switching manifolds of the nonsmooth F(x) in equation (4). Red isolated solution represents the limit cycle and red dots indicate the equilibria of the model. Black dots around the perimeter represent ICs.

Based on the location of the equilibria and the switching manifolds, we can conclude that one equilibrium occurs when the firing rates of both ODE equations are equal to zero and the second equilibrium occurs when both firing rates take on the value $\frac{\varepsilon}{4}x + \frac{1}{2}$. Because of this, we can analyze them by applying standard stability theories.

When both firing rates are zero, the equilibrium point $(u_1, v_1) = (0,0)$ can be calculated by inspection. When both firing rates are equal to $\frac{\varepsilon}{4}x + \frac{1}{2}$, the equilibrium (u_2, v_2) can be calculated by solving,

$$\begin{aligned} \dot{u} &= -u_2 + \frac{\varepsilon}{4}(I_u + w_{uu}u_2 - w_{vu}v_2) + \frac{1}{2} = 0, \\ \dot{v} &= -v_2 + \frac{\varepsilon}{4}(I_v + w_{uv}u_2 - w_{vv}v_2) + \frac{1}{2} = 0, \end{aligned} \tag{42}$$

which simplifies to the following system of equations:

$$\begin{aligned} \left(w_{uu} - \frac{4}{\varepsilon}\right) \cdot u_2 - (w_{vu}) \cdot v_2 &= -I_u - \frac{2}{\varepsilon}, \\ (w_{uv}) \cdot u_2 - \left(w_{vv} + \frac{4}{\varepsilon}\right) \cdot v_2 &= -I_v - \frac{2}{\varepsilon}. \end{aligned} \tag{43}$$

To numerically solve this system of equations, we plugged in the parameter values found in Table 1, to get the system of equations:

$$\begin{aligned} \left(1 - \frac{4}{100}\right) \cdot u_2 - (2) \cdot v_2 &= -(-0.05) - \frac{2}{100}, \\ 1 \cdot u_2 - \left(0.25 + \frac{4}{100}\right) \cdot v_2 &= -(-0.3) - \frac{2}{100}, \end{aligned} \tag{44}$$

which results in the equilibrium,

$$(u_2, v_2) = (0.32, 0.14).$$

According to the phase portrait in Figure 32, there is a limit cycle surrounding the equilibrium point (u_2, v_2), as marked by the red curve. In general, the stability of a limit cycle is difficult to analytically identify. Thus, any future conclusions made

about this invariant set are based on the behavior of nearby solutions (i.e. the numerical solutions).

Based on the phase portrait in Figure 32, we grouped trajectories based on the invariant set each one approached. These groups are known as the basins of attraction, which indicate the regions of initial conditions that approach the specific invariant set as time moves forward. The basins of attraction of the Nonsmooth Wilson-Cowan model are shown in Figure 33, where the blue region corresponds to the basin of attraction of the equlibrium (u_1, v_1) and the green region corresponds to the basin of attraction of the limit cycle. This figure confirms the fact that the initial conditions within Regions 1, 2, and 3 exhibit no spiking behavior of the states since they approach the origin, while initial conditions within Regions 4, 5, and 6 approach the limit cycle, so spiking behavior is present.

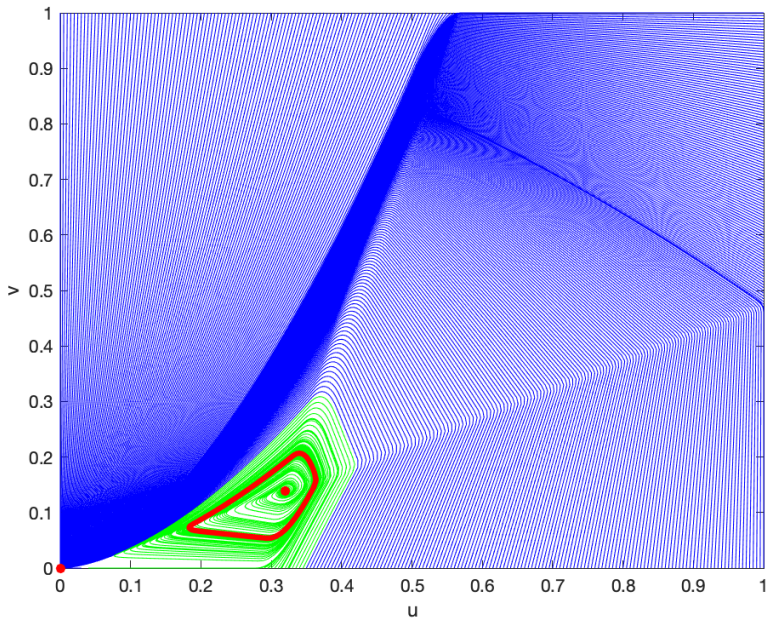

Figure 33: Basins of attraction of the Nonsmooth Wilson-Cowan model. Solutions in blue are approaching the origin while solutions in green are approaching the limit cycle.

When comparing Figure 33 with the heatmap of Figure 12, it is clear to see that the basins of attraction closely resemble the different regions of sensitivity behavior. The parametric influence to the Wilson-Cowan model with initial conditions in Regions 1, 2, and 3 are weaker than those in Regions 4, 5, and 6. This is due to these regions having limited state variable activity, which corresponds to the region of initial conditions that approach the origin over time; therefore, the initial conditions within Regions 1, 2, and 3 are part of the basin of attraction of the equilibrium point $(u_1, v_1) = (0,0)$, while initial conditions within Regions 4, 5, and 6 are part of the basin of attraction of the limit cycle. Thus the model's sensitivity for a specific initial condition must be dependent on the basin of attraction.

Long-Term Behavior of the Nonsmooth Model

The stability of an equilibrium point provides information about the long-term behavior of nearby solutions. As shown in Figure 32, trajectories approach the point $(u_1, v_1) = (0,0)$ and the limit cycle, but are repelled from the point $(u_2, u_2) = (0.32, 0.14)$. Based on the standard stability theories explained in Chapter II, we would hypothesize that the point $(u_1, v_1) = (0,0)$ and the limit cycle are asymptotically stable, while the point $(u_2, u_2) = (0.32, 0.14)$ is unstable. To verify these conjectures we can linearize the ODE systems by calculating the Jacobian matrix of the right-hand side functions and analyze its eigenvalues at each equilibrium. The Jacobian matrix is calculated by,

$$J_x f(p_0, x) = \begin{bmatrix} \frac{\partial (f_u)}{\partial u} & \frac{\partial (f_u)}{\partial v} \\ \frac{\partial (f_v)}{\partial u} & \frac{\partial (f_v)}{\partial v} \end{bmatrix}, \tag{45}$$

for parameter values p_0 found in Table 1 where f_u and f_v are the right-hand side functions of the Wilson-Cowan model in equation (22) with nonsmooth firing rate function in equation (25) with respect to u and v respectively.

Since the nonsmooth parts of the Wilson-Cowan model are the switching manifolds and neither (u_1, v_1) nor (u_2, v_2) is located on these lines, they can be analyzed using standard theory. As explained above, the equlibrium point $(u_1, v_1) = (0,0)$ occurs when both firing rates are zero. Thus we have,

$$J_x f(p_0, u_1, v_2) = \begin{bmatrix} \frac{\partial(-u)}{\partial u} & \frac{\partial(-u)}{\partial v} \\ \frac{\partial(-\frac{v}{\tau})}{\partial u} & \frac{\partial(-\frac{v}{\tau})}{\partial v} \end{bmatrix} = \begin{bmatrix} -1 & 0 \\ 0 & -\frac{1}{\tau} \end{bmatrix}. \tag{46}$$

This is a diagonal matrix, thus it has eigenvalues $\lambda_1 = -1$ and $\lambda_1 = -\frac{1}{\tau}$. The real part of these values are negative (since the timescale constant τ is positive), which confirms that the equilibrium point $(u_1, v_1) = (0,0)$ is asymptotically stable.

The equilibrium point $(u_2, v_2) = (0.32, 0.14)$ occurs when both firing rates are equal to the second input of the mid function. Therefore, the Jacobian matrix is

$$\begin{aligned} J_x f(p_0, u_2, v_2) &= \begin{bmatrix} \frac{\partial(-u+\frac{\varepsilon}{4}(I_u+w_{uu}u-w_{vu}v)+\frac{1}{2})}{\partial u} & \frac{\partial(-u+\frac{\varepsilon}{4}(I_u+w_{uu}u-w_{vu}v)+\frac{1}{2}))}{\partial v} \\ \frac{\partial(-v+\frac{\varepsilon}{4}(I_v+w_{uv}u-w_{vv}v)+\frac{1}{2}))+\frac{1}{2})}{\partial u} & \frac{\partial(-v+\frac{\varepsilon}{4}(I_v+w_{uv}u-w_{vv}v)+\frac{1}{2}))}{\partial v} \end{bmatrix} \\ &= \begin{bmatrix} -1+\frac{\varepsilon}{4}(w_{uu}) & -\frac{\varepsilon}{4}(w_{vu}) \\ \frac{\varepsilon}{4}(w_{uv}) & -1-\frac{\varepsilon}{4}(w_{vv}) \end{bmatrix} \\ &= \begin{bmatrix} 24 & -50 \\ 25 & \frac{21}{4} \end{bmatrix}. \end{aligned} \tag{47}$$

Using MATLAB, we calculated the eigenvalues of this matrix to be $\lambda_1 = 14.625 + 34.0897i$ and $\lambda_2 = 14.625 - 34.0897i$. Since the real part of at least one eigenvalue is positive, we can confirm that $(u_2, v_2) = (0.32, 0.14)$ is unstable.

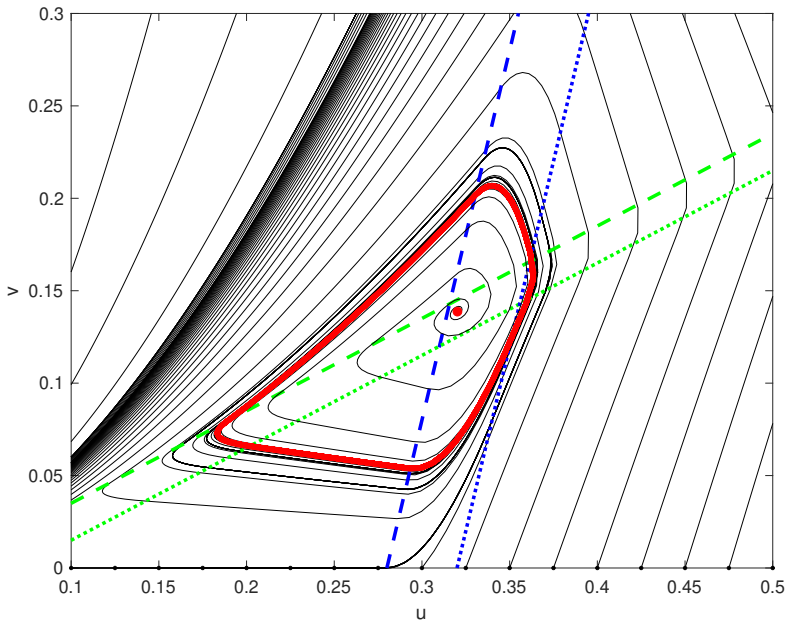

Figure 34: Limit cycle of the Nonsmooth Wilson-Cowan model. Blue and green dashed lines represent the switching manifolds. Red isolated solution is the limit cycle and red dot is an equilibrium.

Since the limit cycle crosses the switching manifolds, standard stability theories fail. Having said that, nearby solutions approach the limit cycle, as shown in Figure 34, which displays the phase portrait of the nonsmooth model in a zoomed-in window. Thus, we expect the limit cycle to be asymptotically stable.

Comparison to Stability Analysis of Smooth Model

To compare the nonsmooth model to the smooth Wilson-Cowan model, we plotted the phase portrait of the smooth model (see Figure 35). The results show that all trajec-

tories of the smooth model spiral towards a limit cycle similar to the one found in the Nonsmooth Wilson-Cowan model as shown in Figure 32. Since all trajectories are approaching this cycle, the solutions that are initialized within the limit cycle must be moving away from a point inside of this cycle, indicating the existence of an unstable equilibrium (both invariant sets are shown in red). We will denote the equilibrium inside the limit cycle as (u^*, v^*), where the asterisk implies it is an equilibrium of the Smooth Wilson-Cowan model. This figure also shows solutions approach the point $(u, v) = (0, 0)$ for a period of time, but do not remain nearby this point for all t. Instead, solutions approach the limit cycle as $t \to \infty$ which is unlike the long-term state behavior of the nonsmooth model.

To confirm the point $(u, v) = (0, 0)$ is not an equilibirum of the smooth model, we calculated the right-hand side equations of the model at this point. Then we have,

$$f_u(p, 0, 0) = -u + \frac{1}{1 + e^{-\varepsilon(I_u + w_{uu}(0) - w_{vu}(0))}} = 0.006692,$$
$$f_v(p, 0, 0) = -v + \frac{1}{1 + e^{-\varepsilon(I_u + w_{uv}(0) - w_{vv}(0))}} = 9.357 \times 10^{-14},$$

which indicates the origin does not satisfy the requirements of a fixed point and is not an equilibrium of the Smooth Wilson-Cowan model. Therefore, there is an equilibrium present in the nonsmooth model that is not present in the smooth one, supporting the difference in state variable behavior discussed in Chapter IV.

The above calculation confirmed that the smooth model has a single equilibrium point, (u^*, v^*), located within the limit cycle. This equilibrium can be calculated using

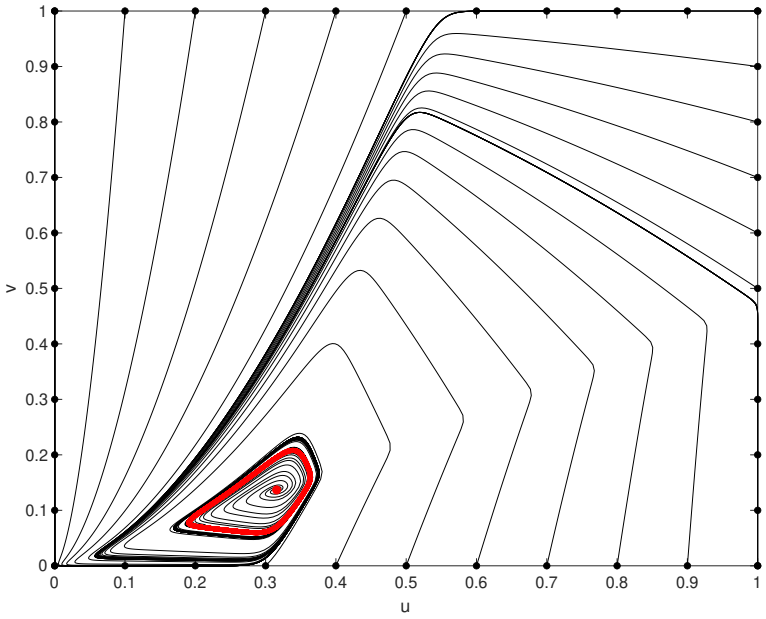

Figure 35: Phase portrait of the Smooth Wilson-Cowan model. Red isolated solution represents the limit cycle and red dots indicate the equilibria of the model. Black dots around the perimeter represent ICs.

equation (40) with $F(x) = \text{expit}(x)$. Then we have,

$$\begin{aligned} 0 &= -u^* + \text{expit}(I_u + w_{uu}u^* - w_{vu}v^*), \\ 0 &= -v^* + \text{expit}(I_u + w_{uv}u^* - w_{vv}v^*). \end{aligned} \tag{48}$$

Further calculations using MATLAB allowed us to numerically determine that $(u^*, v^*) = (0.32, 0.14)$, which equals the equilibrium (u_2, v_2) from the Nonsmooth Wilson-Cowan model.

Similarly to the nonsmooth model, we grouped solutions of the model based on the invariant set they approach as time moves forward (see Figure 36), which are the basins of attraction. This figure shows that all solutions approach the limit cycle, which supports the fact that spiking behavior is present in all regions of the smooth model.

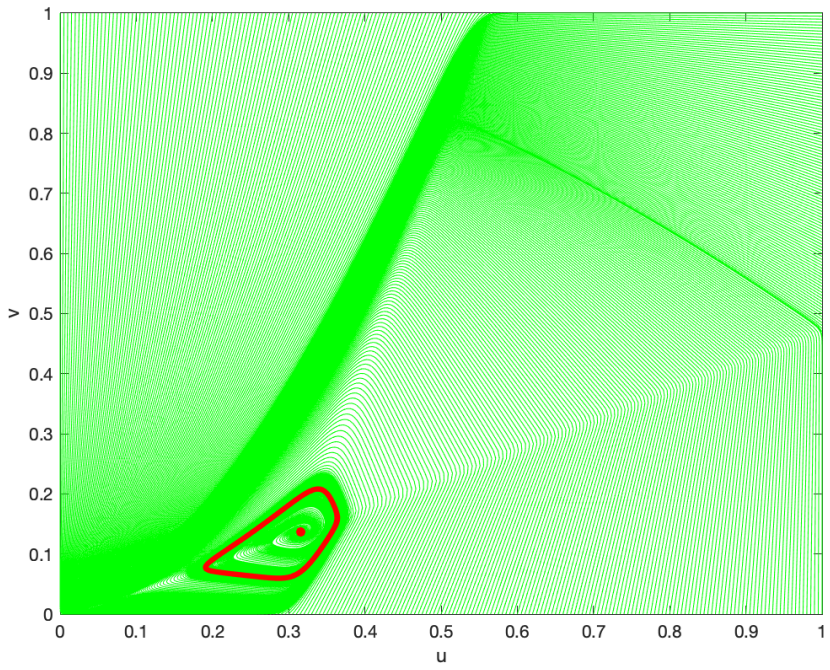

Figure 36: Basins of attraction of the Smooth Wilson-Cowan model. Solutions in green are approaching the limit cycle.

To verify the stability of the equilibrium of the smooth model, we can investigate the eigenvalues of the Jacobian of the right-hand side equations of the smooth model, which is calculated by,

$$J_x f^*(p_0, x) = \begin{bmatrix} \frac{\partial(f_u^*)}{\partial u} & \frac{\partial(f_u^*)}{\partial v} \\ \frac{\partial(f_v^*)}{\partial u} & \frac{\partial(f_v^*)}{\partial v} \end{bmatrix}, \tag{49}$$

where f_u^* and f_v^* are the right-hand side functions of the Wilson-Cowan model in equation (22) with smooth firing rate function in equation (23) with respect to u and v respectively.

We can then use the Jacobian of equation (49) to find the eigenvalues of the matrix with respect to the smooth equilibrium point, $(u^*, v^*) = (0.32, 0.14)$ by plugging this point in. Then we have,

$$J_x f^*(p_0,u^*,v^*) = \begin{bmatrix} -\frac{\varepsilon w_{uu} e^{-\varepsilon(I_u+w_{uu}(0.32)-w_{vu}(0.14))}}{(1+e^{-\varepsilon(I_u+w_{uu}(0.32)-w_{vu}(0.14))})^2} & -\frac{\varepsilon w_{vu} e^{-\varepsilon(I_u+w_{uu}(0.32)-w_{vu}(0.14))}}{(1+e^{-\varepsilon(I_u+w_{uu}(0.32)-w_{vu}(0.14))})^2} \\ \frac{\varepsilon w_{uv} e^{-\varepsilon(I_v+w_{uv}(0.32)-w_{vv}(0.14))}}{\tau(1+e^{-\varepsilon(I_v+w_{uv}(0.32)-w_{vv}(0.14))})^2} & -\frac{1}{\tau} - \frac{\varepsilon w_{vv} e^{-\varepsilon(I_v+w_{uv}(0.32)-w_{vv}(0.14))}}{\tau(1+e^{-\varepsilon(I_v+w_{uv}(0.32)-w_{vv}(0.14))})^2} \end{bmatrix}$$
$$= \begin{bmatrix} -19.661 & -39.322 \\ 24.858 & -7.881 \end{bmatrix}. \tag{50}$$

Using MATLAB we then calculated the eigenvalues of this matrix to be $\lambda = 5.890 + 28.0682i$ and $\lambda = 5.890 - 28.0682i$. Since the real part of at least one eigenvalue is positive, the equilibrium point $(u^*, v^*) = (0.32, 0.14)$ is unstable.

As stated previously, the limit cycle of the smooth Wilson-Cowan model is complicated enough that we could not analytically identify it. However, as shown in Figure 37, all nearby trajectories approach the origin, then after a period of time they approach the limit cycle. Therefore, we expect it to be "attractive" which indicates solutions approach the invariant set as $t \to \infty$. Note that the limit cycle does not seem to be asymptotically stable, as it is in the nonsmooth model, since nearby solutions of the smooth model first move away from the limit cycle and towards the origin. After a period of time, these solutions then approach the cycle, indicating it is attractive, but cannot be described as asymptotically stable. This behavior is unique to the smooth case, as nearby solutions to the limit cycle of the nonsmooth model approach the cycle itself, indicating the cycle is asymptotically stable.

As we did for the nonsmooth model, we compared the basins of attraction to the heatmap displaying the parametric influence over a range of ICs of the Smooth Wilson-

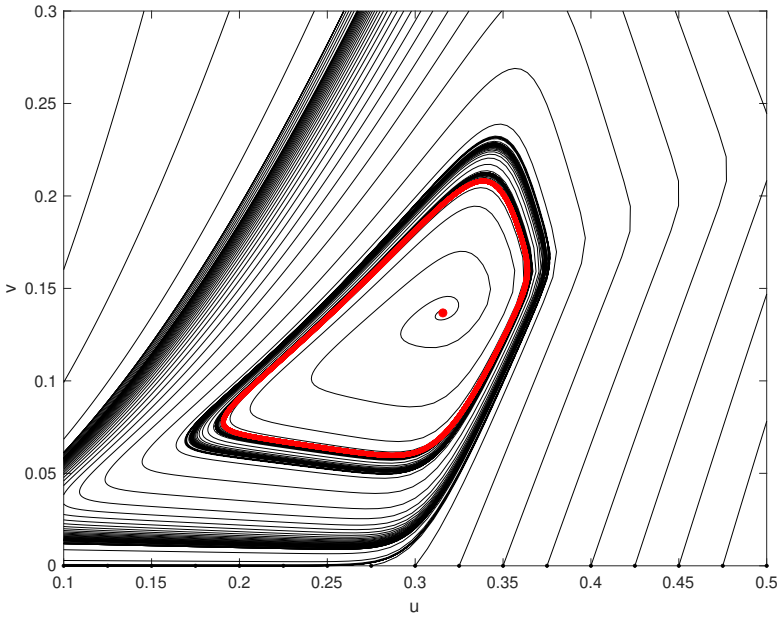

Figure 37: Limit cycle of the Smooth Wilson-Cowan Model. Red isolated solution is the limit cycle and red dot represents an equilibrium.

Cowan model (see Figure 20). We found that these images appear to be similar, since there is one basin of attraction in the smooth model and there is primarily one region of distinct sensitivity behavior. This is a similar observation to the one we made about the nonsmooth basins of attraction in comparison to the heatmap of the nonsmooth model. Though the smooth model is less sensitive than the nonsmooth model overall, there is still a notable level of parametric influence in each region, which results in homogeneous levels of model sensitivity across all ICs.

Taking a closer look at the long-term behavior of the states of the smooth model reveals the fact that there is a spiking behavior exhibited for all ICs, indicating a high level of neural activity. The spiking behavior of the states for each region is reflected by the basin of attraction, since all solutions approach the asymptotically stable limit cycle. Based on these observations, we hypothesize that the sensitivity of the Wilson-Cowan

model is dependent on the long-term behavior of the states. This conclusion supports our findings that the model is relatively insensitive to the model parameters for ICs that exhibit low state variable activity, such as regions 1, 2, and 3 of the nonsmooth model, and is notably sensitive to parameters for ICs where the states exhibit a spiking behavior, such as regions 4, 5, and 6 of the nonsmooth model and all regions of the smooth model.

Though we can make the above conlusion about the Wilson-Cowan model as a whole, the differences between the stability analysis of the nonsmooth model and the smooth model supports the need to analyze nonsmooth firing rates in regards to the Wilson-Cowan model. The most significant difference between the two models is that there is an equilibrium present in the nonsmooth model that is not present in the smooth model. Since the origin is not an equilibrium in the smooth model and the limit cycle attracts all trajectories, this implies both state variables exhibit spiking behavior for all initial conditions. However, this means that neurons in the brain are in constant communication no matter how many neurons are initially active, which gives rise to questions about how biologically accurate each model is.

CHAPTER VI

Conclusion

Based on the results of Chapter V, it is apparent that the Nonsmooth Wilson-Cowan model is most sensitive to specific problem parameters depending on what ICs, (u_0, v_0), are used. For the initial conditions within Regions 1, 2, and 3, the model is most sensitive to the initial conditions u_0 and v_0, yet is relatively insensitive to all parameters. In these regions, the state variables exhibit no spiking behavior, which we assume implies there is a lower amount of neural activity. However, once the initial conditions cross over into Regions 4, 5, and 6, the state variables begin to spike, which would imply there is a higher amount of neural activity. Thus, perturbations of the initial conditions influence the level of neural activity exhibited by the states of the Nonsmooth Wilson-Cowan model, supporting a higher influence from the these parameters in regions of low neural activity.

Having said that, for ICs in Regions 1, 2, and 3, the nonsmooth model is influenced by the initial conditions at a very low level. Overall, for ICs in regions of low neural activity, there is an insignificant amount of parametric influence to the nonsmooth model. Based on these observations, we hypothesize that when the state variables exhibit no spiking behavior, the Nonsmooth Wilson-Cowan model is relatively insensitive to all model parameters.

On the other hand, for ICs within Regions 4, 5, and 6, there are significant levels of parametric influence, which indicates the nonsmooth model is more sensitive in the areas. According to the sensitivity analysis of the nonsmooth model, the most influential parameter of these regions is the timescale constant, τ. This parameter is necessary to the model since the excitatory and inhibitory neuron populations function on different timescales. Inhibitory neurons fire more quickly than excitatory neurons, so the timescale constant must reflect a faster firing rate within this population in order to create a more biologically accurate representation of this neural network. In order to achieve this, the timescale constant is assumed to be less than one (note that $\tau = 1$ would indicate both populations are functioning on the same timescale). The finding that τ is the most influential parameter for these regions of the nonsmooth model is unsurprising, since inhibitory neurons prevent receiving neurons from firing. If these neurons are firing more quickly, a higher level of inhibition than excitation is present in the network, resulting in a decrease in the proportion of firing neurons in both populations. Thus decreasing τ, which increases the firing rate of inhibitory neurons, would decrease the level of neural activity in the states and vice versa. This phenomenon is reflected in the results of our sensitivity analysis, validating these conclusions.

When comparing the sensitivity analysis of the Nonsmooth Wilson-Cowan model to the analysis of the Smooth Wilson-Cowan model, we found that the state variable behavior of both models are relatively similar, while the sensitivities of both models differ. This indicates that the nonsmooth model may be a good representation of the smooth, but the most influential parameters to the one model are not the most influential to the other. In fact, the smooth model seems to be somewhat sensitive to the model param-

eters for all ICs, while the nonsmooth model is relatively insensitive to all parameters in some regions of ICs and highly sensitive to specific parameters in others. Since the biological motivation of the smooth model has been questioned by some authors [3], these differences might influence conclusions about which model is more biologically accurate. Overall, the results of this comparison supports the need to analyze nonsmooth forms of the Wilson-Cowan model as different conclusions can be made about the results.

Although similar, the state variable behavior of the smooth and nonsmooth models are not identical. When analyzing both models, it is clear to see that the nonsmooth model exhibits spiking behavior in specific regions, while the state variables of the smooth model spike in all regions of ICs. This difference in behavior raises questions about the long-term behavior of the Wilson-Cowan models, which we attempted to answer with a stability analysis of the smooth and nonsmooth model.

While performing a stability analysis of the Nonsmooth Wilson-Cowan model, we found an asymptotically stable equilibrium at the origin, an unstable equilibrium, and an asymptotically stable limit cycle (similar to the cycle found in [5]). However, the stability analysis of the smooth model resulted in an unstable equilibrium and an attractive limit cycle, but no equilibrium at the origin. The difference in equilibria between the smooth and nonsmooth models led to yet another consideration of how biologically accurate each model is. The fact that there is no equilibrium at the origin of the smooth model indicates that no matter what initial condition is implemented, state variables will exhibit some level of neural activity. However, are there biological scenarios that do not produce ongoing neuron firing? If so, the model should result in

zero neural activity after an amount of time for specific ICs, similar to what we have observed in the nonsmooth model. Having said that, if there truly are no ICs that results in zero neural activity and neurons are constantly firing, then the smooth model would be a more accurate representation of the long-term behavior of the biological phenomenon. Having said that, some authors [27] say that a biologically accurate space-clamped neural network model should not be reactive to small outside inputs. Thus, when there is initially no neuron activity, indicating the only activity present is from outside inputs, there should be no activity for any time. Therefore biologically accurate models should include an asymptotically stable equilibrium point at the origin. Based on this condition, we would hypothesis that the Nonsmooth Wilson-Cowan model is more biologically accurate than the smooth.

The conclusions drawn based on the sensitivity and stability analysis of the nonsmooth model studied in this thesis show a difference in parametric influence and long-term state variable behavior based on an initial ratio of firing excitatory and inhibitory neurons. However, the analyses of the smooth model studied in this thesis show that the initial ratio between these two neuron populations is not as influential to the state variable behavior, given a recurrent spiking behavior for all ICs. Based on these results, there is a possibility that our conclusions could be applied to research on the biological relationship between excitatory and inhibitory neurons in the brain, which is referred to as excitation-inhibition balance (E-I balance). It has been found that an imbalance in the relationship can greatly impact neural activity. For example, a decreased number of inhibitory neurons firing results in a limited amount of inhibition within a neural network, which can cause excitatory neurons to fire uncontrollably [8]. This form of

imbalance is a contributing factor to seizures, which arise if the brain is overstimulated. Thus research on E-I balance applies to studies of neurophsychiatric conditions such as schizophrenia as well as seizure disorders such as epilepsy [23].

In general, studies of neural mass models can provide clarity on how some areas of the brain interact. Further research of the Nonsmooth Wilson-Cowan model can answer questions closely related to this topic through synchronization analysis, which occurs both in normal and abnormal pathological conditions [19]. In addition, an analysis of the full network model of the Wilson-Cowan neural mass model could provide conclusions on neural activity that consider more complex levels of biological phenomenon, such as the spatial structure of an array of neurons. Such analysis can explain some aspects of neurodegenerative diseases that cause damage to the brain's neural connections and therefore synchronization. As explained in [22], examples include Alzheimer's disease, behavioral variant frontotemporal dementia, semantic dementia, progressive nonfluent aphasia, and corticobasal syndrome. We hope to touch on these subjects through future analysis of the Wilson-Cowan model.

REFERENCES

[1] P. I. BARTON, K. A. KHAN, P. STECHLINSKI, AND H. A. J. WATSON, *Computationally relevant generalized derivatives: Theory, evaluation and applications*, Optimization Methods and Software, 33 (2018), pp. 1030–1072.

[2] J. M. BEKKERS, *Pyramidal neurons*, Current Biology, 21 (2011), p. R975.

[3] Á. BYRNE, R. D. O'DEA, M. FORRESTER, J. ROSS, AND S. COOMBES, *Next-generation neural mass and field modeling*, Journal of Neurophysiology, 123 (2020), pp. 726–742.

[4] F. H. CLARKE, *Optimization and Nonsmooth Analysis*, SIAM, Philadelphia, PA, 1990.

[5] S. COOMBES, Y. M. LAI, M. ŞAYLI, AND R. THUL, *Networks of piecewise linear neural mass models*, European Journal of Applied Mathematics, 29 (2018), pp. 869–890.

[6] J. D. COWAN, J. NEUMAN, AND W. VAN DRONGELEN, *Wilson–Cowan equations for neocortical dynamics*, The Journal of Mathematical Neuroscience, 6 (2016), pp. 1–24.

[7] B. ERMENTROUT AND D. H. TERMAN, *Mathematical Foundations of Neuroscience*, vol. 35, Springer, 2010.

[8] C. L. GATTO AND K. BROADIE, *Genetic controls balancing excitatory and inhibitory synaptogenesis in neurodevelopmental disorder models*, Frontiers in Synaptic Neuroscience, 2 (2010), p. 1553.

[9] Q. GU, S. LI, A. KUMAR, J. MURRAY, AND J. GJORGJIEVA, *Neuromatch Academy Computational Neuroscience Course - Tutorial 2: Wilson-Cowan Model*. 2020.

[10] J. HARRIS AND B. ERMENTROUT, *Bifurcations in the wilson–cowan equations with nonsmooth firing rate*, SIAM Journal on Applied Dynamical Systems, 14 (2015), pp. 43–72.

[11] K. A. KHAN AND P. I. BARTON, *Generalized derivatives for solutions of parametric ordinary differential equations with non-differentiable right-hand sides*, Journal of Optimization Theory and Applications, 163 (2014), pp. 355–386.

[12] K. A. KHAN AND P. I. BARTON, *A vector forward mode of automatic differentiation for generalized derivative evaluation*, Optimization Methods and Software, 30 (2015), pp. 1185–1212.

[13] Z. P. KILPATRICK, *Encyclodpeida of Computational Neuroscience: Wilson-Cowan Model*, Springer Verlag, 2013.

[14] L. KUHLMANN, D. R. FREESTONE, J. H. MANTON, B. HEYSE, H. E. VEREECKE, T. LIPPING, M. M. STRUYS, AND D. T. LILEY, *Neural mass model-based tracking of anesthetic brain states*, NeuroImage, 133 (2016), pp. 438–456.

[15] T. B. LUKE, E. BARRETO, AND P. SO, *Complete classification of the macroscopic behavior of a heterogeneous network of theta neurons*, Neural Computation, 25 (2013), pp. 3207–3234.

[16] Y. NESTEROV, *Lexicographic differentiation of nonsmooth functions*, Mathematical Programming, 104 (2005), pp. 669–700.

[17] W. NICOLA AND S. A. CAMPBELL, *Mean-field models for heterogeneous networks of two-dimensional integrate and fire neurons*, Frontiers in Computational Neuroscience, 7 (2013), p. 184.

[18] ——, *Nonsmooth bifurcations of mean field systems of two-dimensional integrate and fire neurons*, SIAM Journal on Applied Dynamical Systems, 15 (2016), pp. 391–439.

[19] ——, *Normalized connectomes show increased synchronizability with age through their second largest eigenvalue*, SIAM Journal on Applied Dynamical Systems, 20 (2021), pp. 1158–1176.

[20] L. PERKO, *Differential Equations and Dynamical Systems*, vol. 7, Springer Science & Business Media, 2013.

[21] S. SCHOLTES, *Introduction to Piecewise Differentiable Equations*, Springer, New York, 2012.

[22] W. W. SEELEY, R. K. CRAWFORD, J. ZHOU, B. L. MILLER, AND M. D. GREICIUS, *Neurodegenerative diseases target large-scale human brain networks*, Neuron, 62 (2009), pp. 42–52.

[23] V. S. SOHAL AND J. L. RUBENSTEIN, *Excitation-inhibition balance as a framework for investigating mechanisms in neuropsychiatric disorders*, Molecular Psychiatry, 24 (2019), pp. 1248–1257.

[24] S. H. STROGATZ, *Nonlinear Dynamics and Chaos: with Applications to Physics, Biology, Chemistry, and Engineering*, CRC press, 2018.

[25] H.-A. TSENG AND X. HAN, *Distinct spiking patterns of excitatory and inhibitory neurons and lfp oscillations in prefrontal cortex during sensory discrimination*, Frontiers in Physiology, 12 (2021), p. 618307.

[26] Y. WEN, Z. DONG, J. LIU, P. AXERIO-CILIES, Y. DU, J. LI, L. CHEN, L. ZHANG, L. LIU, J. LU, ET AL., *Glutamate and gabaa receptor crosstalk mediates homeostatic regulation of neuronal excitation in the mammalian brain*, Signal Transduction and Targeted Therapy, 7 (2022), p. 340.

[27] H. R. WILSON, *Spikes, Decisions, and Actions: the Dynamical Foundations of Neuroscience*, Oxford University Press, 1999.

[28] H. R. WILSON AND J. D. COWAN, *A mathematical theory of the functional dynamics of cortical and thalamic nervous tissue*, Kybernetik, 13 (1973), pp. 55–80.

[29] L. H. ZETTERBERG, L. KRISTIANSSON, AND K. MOSSBERG, *Performance of a model for a local neuron population*, Biological Cybernetics, 31 (1978), pp. 15–26.

AUTHOR'S BIOGRAPHY

Cadi Howell was born in Cambridge, England on December 5, 2001, and raised on Mount Desert Island, Maine. Cadi will earn a Bachelor of Science in mathematics with a minor in neuroscience in May 2024 and is currently on track to earn a masters in mathematics through the University of Maine's 4+1 program come May 2025. She has been a member of the UMaine Women's Club Soccer Team for the last four years. In her third year, she was voted to be the Club's Secretary and during her fourth year she became the Vice President. Cadi plans to continue her work analyzing Neural Mass Models throughout her final year as a graduate student and hopes to pursue a career in mathematical/biological modeling and analysis.